Atmospheric
Chemistry
and Physics
Discussions

Impact of particle number and mass size distributions of major chemical components on particle mass scattering efficiency in urban Guangzhou of South China

Jun Tao[1,*], Zhisheng Zhang[1], Yunfei Wu[2], Leiming Zhang[3,*], Zhijun Wu[4], Peng Cheng[5], Mei Li[5], Laiguo Chen[1], Renjian Zhang[2], Junji Cao[6]

[1]South China Institute of Environmental Sciences, Ministry of Environmental Protection, Guangzhou, China

[2]RCE-TEA, Institute of Atmospheric Physics, Chinese Academy of Sciences, Beijing, China

[3]Air Quality Research Division, Science and Technology Branch, Environment and Climate Change Canada, Toronto, Canada

[4]State Key Joint Laboratory of Environmental Simulation and Pollution Control, College of Environmental Sciences and Engineering, Peking University, Beijing, China

[5]Institute of Mass Spectrometer and Atmospheric Environment, Jinan University, Guangzhou, China

[6]Key Laboratory of Aerosol Chemistry and Physics, Institute of Earth Environment, Chinese Academy of Sciences, Xi'an, China

*Correspondence to: (Leiming Zhang) leiming.zhang@canada.ca or (Jun Tao) taojun@scies.org

Atmospheric
Chemistry
and Physics
Discussions

1   **Abstract.** To grasp the key factors affecting particle mass scattering efficiency

2   (MSE), particle mass and number size distribution, bulk $PM_{2.5}$ and PM_{10} and their

3   major chemical compositions, and particle scattering coefficient (b_{sp}) under dry

4   condition were measured at an urban site in Guangzhou, south China during

5   2015-2016. On annual average, $10\pm2\%$, $48\pm7\%$ and $42\pm8\%$ of PM_{10} mass were in the

6   condensation, droplet and coarse modes, with mass median aerodynamic diameters

7   (MMADs) of 0.21 ± 0.00, 0.78 ± 0.07 and 4.57 ± 0.42 μm, respectively. The identified

8   chemical species mass concentrations can explain $79\pm3\%$, $82\pm6\%$ and $57\pm6\%$ of the

9   total particle mass in the condensation, droplet and coarse mode, respectively. Organic

10   matter (OM) and elemental carbon (EC) in the condensation mode, OM, $(NH_4)_2SO_4$,

11   NH_4NO_3 and crustal element oxides in the droplet mode, and crustal element oxides,

12   OM and $CaSO_4$ in the coarse mode were the dominant chemical species in their

13   respective modes. The measured b_{sp} can be reconstructed to the level of $91\pm10\%$

14   using Mie theory with input of the estimated chemically-resolved number

15   concentrations of NaCl, $NaNO_3$, Na_2SO_4, NH_4NO_3, $(NH_4)_2SO_4$, K_2SO_4, $CaSO_4$,

16      $Ca(NO_3)_2$, OM, EC, crustal element oxides and unidentified fraction. MSEs of bulk

17   particle and individual chemical species were underestimated by less than 13 % in any

18   season based on the estimated b_{sp} and chemical species mass concentrations. Seasonal

19   average MSEs varied in a small range of 3.5 ± 0.1 to 3.9 ± 0.2 m^2 g^{-1} for fine particles,

20   which was mainly caused by seasonal variations of the mass fractions and MSEs of

21   OM in the droplet mode.

22   Keywords: particle size distribution, particle chemical composition, particle mass

23   scattering efficiency

Atmospheric
Chemistry
and Physics
Discussions

Open Access

1. Introduction

24

25   Light extinct coefficient (b_{ext}) of atmospheric particles, which is the sum of their

26   scattering (b_{sp}) and absorption (b_{ap}) coefficients, is a key index of haze weather (Hand

27   and Malm, 2007). In most cases, b_{sp} accounted for more than 90% of b_{ext} (Takemura

28   et al., 2002; Tao et al., 2017a). Numerous studies have demonstrated that haze is

29   mainly caused by high concentrations of fine particles (PM$_{2.5}$, with aerodynamic

30   diameter smaller than 2.5 μm) (Hand and Malm, 2007; Huang et al., 2012; Malm et

31   al., 1994; Malm et al., 2000; Malm et al., 2003; Malm and Hand, 2007; Sisler and

32   Latimer, 1993; Sisler et al., 1996; Sisler and Malm, 2000; Wang et al., 2014b; Zhao et

33   al., 2013). Knowledge of the dominant chemical species in PM$_{2.5}$ (e.g. $(NH_4)_2SO_4$,

34   NH_4NO_3 and OM) and their contributions to b_{sp} is crucial in making feasible policies

35   for alleviating haze (Watson, 2002).

36   Generally, b_{sp} can be estimated in reasonable accuracy using Mie theory when

37   size distributions of dominant chemical species are known (Cheng et al., 2008; Cheng

38   et al., 2009; Gao et al., 2015; Malm et al., 2003; Watson et al., 2008). However,

39   routinely monitoring of the size distributions of all the dominant chemical

40   components is impractical. To evaluate haze in the national parks in U.S.A. under the

41   Regional Haze Rule, the original and revised IMPROVE formulas were developed for

42   reconstructing b_{sp} based on the chemical species in PM$_{2.5}$ and coarse particle mass

43   concentrations monitored in the IMPROVE network (Pitchford et al., 2007; Watson,

44   2002). The MSEs of chemical species are the important parameters of the IMPROVE

45   formulas for building the relationships between chemical species and b_{sp} (Hand and

Atmospheric
Chemistry
and Physics
Discussions

46   Malm, 2007). The recommended MSEs of $(NH_4)_2SO_4$, NH_4NO_3, OM and fine soil

47   (estimated from crustal elements) in $PM_{2.5}$ were 3.0, 3.0, 4.0 and 1.0 m^2 g^{-1},

48   respectively, in the original IMPROVE formula. However, MSEs of any particle

49   species vary with its mass concentrations and size distributions (Lowenthal and

50   Kumar, 2004; Malm et al., 2003; Malm and Hand, 2007; Malm and Pitchford, 1997).

51   Subsequently, the MSEs and mass concentrations of $(NH_4)_2SO_4$, NH_4NO_3 and OM in

52   the $PM_{2.5}$ were separated into small and large modes in the revised IMPROVE

53   formula (Hand and Malm, 2007).

54   China has been suffering from severe $PM_{2.5}$ pollution and haze weather (Li et al.,

55   2016; Ming et al., 2017; Wang et al., 2017; Zhang et al., 2013). To investigate the

56   formation of haze, the original and revised IMPROVE formulas have been directly

57   applied in many cities in China (Hua et al., 2015; Shen et al., 2014; Tao et al., 2009;

58   Zhang et al., 2012a; Zou et al., 2018). The IMPROVE formulas have been proved to

59   over- or underestimate b_{sp} in urban cities in China (Cao et al., 2012; Cheng et al.,

60   2015; Han et al., 2014; Jung et al., 2009a; Jung et al., 2009b; Tao et al., 2012; Tao et

61   al., 2014b), which were likely due to the significantly different size distributions of

62   the major chemical components and related mass fractions in $PM_{2.5}$ between different

63   countries or even cities (Bian et al., 2014; Cabada et al., 2004; Chen et al., 2017; Guo

64   et al., 2009; Lan et al., 2011; Tian et al., 2014b; Yao et al., 2003; Yu et al., 2010;

65   Zhang et al., 2008; Zhuang et al., 1999b). To reduce the uncertainties in the estimated

66   b_{sp} using the original and revised IMPROVE formulas, the average MSEs of

67   dominant chemical species were typically estimated by the multiple linear regression

Atmospheric
Chemistry
and Physics
Discussions

68   method (Hand and Malm, 2007). Although the estimated b_{sp} by the multiple linear

69   regression model may be close to the measured b_{sp}, the rationality of the estimated

70   MSEs of chemical species were unknown (Tao et al., 2014a; Tao et al., 2014b; Tao et

71   al., 2015; Tao et al., 2016; Yao et al., 2010; Wang et al., 2014a).

72   According to Mie theory, variations in size distributions (e.g. MMADs and mass

73   fractions) of chemical components are the most important factors for hindering the

74   applications of the IMPROVE formulas and multiple linear regression models.

75   Although many studies have conducted on understanding size distributions and

76   chemical compositions of fine particles in China, few studies have explored the

77   relationship between the size distribution of major chemical species and their MSEs

78   (Cheng et al., 2008; Cheng et al., 2009; Gao et al., 2015). To fill this knowledge gap,

79   size-segregated particle mass, PM_{10}, $PM_{2.5}$ and their major chemical components, and

80   online data including size distribution of particle number, b_{sp} under dry conditions and

81   water-soluble inorganic ions were synchronously measured at an urban site in

82   Guangzhou covering four seasons in 2015-2016. Size distributions of dominant

83   chemical components were first characterized in section 3.1, followed by discussions

84   on the closures of particle mass and number concentration and b_{sp} in 3.2. Key factors

85   controlling the variations of chemical species and their MSEs were then discussed in

86   section 3.3. Knowledge gained from the present study will improve the assessments of

87   air-quality and climate impact caused by atmospheric particles.

88   **2. Methodology**

89   **2.1 Site description**

90   The observational site in urban Guangzhou is situated inside the South China

Atmospheric
Chemistry
and Physics
Discussions

Open Access

EGU

91   Institute of Environmental Science (SCIES) (23°07′N, 113°21′E) (Fig. 1) with no

92   obvious surrounding industrial activities. The instruments used in this study were

93   installed on the roof of a building 50 m above ground (Tao et al., 2018). The working

94   conditions of all the instruments were controlled under 26 degree in temperature and

95   40% in relative humidity by three air conditioners.

96

97   *Insert Figure 1*

98

99   **2.2 Field sampling**

100   Size-segregated particle samples were collected using Anderson 8-stage air

101   samplers with the cut-off points of 0.43, 0.65, 1.1, 2.1, 3.3, 4.7, 5.8 and 9.0 μm

102   (Thermo-electronic Company, USA). Two sets of samplers were used alternatively

103   due to the need of daily clearance of the instruments. The samplers were operated at

104   an airflow rate of 28.3 L min^{-1}. The sampling flow rate was controlled by a flow meter

105   (Aalborg Inc., USA). Samples were collected on 81 mm quartz fiber filter (Whatman

106   QM-A). Samples were collected during different seasons: 15 July- 6 August, 2015

107   (representative of summer), 15 October- 5 November, 2015 (autumn), 4-20 January,

108   2016 and 19-22 February, 2016 (winter), and 8-20 April, 2016 and 4-14 May, 2016

109   (spring). Sampling duration was 48 h in spring and 24 h in the other seasons, all

110   starting at 10:00 local time.

111   Bulk $PM_{2.5}$ and PM_{10} samples were collected using two Gravisol Sequential

112   Ambient Particulate Monitor (GSAPM) samplers (APM Inc., Korea) at a flow rate of

113   16.7 L min^{-1}. Samples were collected on 47 mm quartz fiber filter (Whatman QM-A).

114   Sampling durations were the same as those for collecting size-segregated samples in

115   every season. The sampling information is summarized in Table 1. Moreover, 8 sets of

116 blank samples were also collected for each of the size-segregated particle, $PM_{2.5}$ and

117 PM_{10} samples during the whole sampling period. The aerosol-loaded filter samples

118 were stored in a freezer at -18 °C before analysis to prevent volatilization of particles.

119

120 *Insert Table 1*

121

122 The background water-soluble inorganic ions (WSII) (e.g. Na^+, Ca^{2+}) of quartz

123 fiber filter were slightly high in general. Thus, 47mm and 81mm quartz fiber filters

124 were first baked at 500 °C for 3 h to remove adsorbed organic vapors; they were then

125 soaked in distilled-deionized water for 3 h for several times to remove WSII until the

126 background values were less than 0.01 mg L^{-1}. Finally, the quartz fiber filters were

127 dried through baking at 200 °C. All blank quartz fiber filters were stored in

128 desiccators.

129 Particle number concentration for particles in the range of 14 nm - 615 nm in

130 mobility diameter (default as geometric diameter (D_g)) was measured using a

131 scanning mobility particle sizer (SMPS; TSI Model 3936, TSI, Inc., St. Paul, MN)

132 combined with a long differential mobility analyzer (DMA; TSI Model 3080) and a

133 condensation particle counter (CPC; TSI Model 3010), and for particles in the range

134 of 542 nm - 10 µm aerodynamic diameter (D_a) using an Aerodynamics Particle Sizer

135 (APS; TSI Model 3321), both at 5 min resolution. Dry b_{sp} was measured using a

136 single wavelength integrating nephelometer (Ecotech Pty Ltd, Australia, Model

137 Aurora1000G) at the wavelength of 520 nm. Ambient air passed through three total

138 suspended particulate (TSP) cyclones, then stainless steel tubes and the Nafion driers

139 prior to sampling by the SMPS, APS and nephelometer. RH of aerosol samples was

140 controlled to be lower than 30% by sweeping dry air from a compressed air pump.

Atmospheric
Chemistry
and Physics
Discussions

141   Water-soluble inorganic ion (NO_3^-) was measured using an In-situ instrument of Gas

142   and Aerosol Composition (IGAC, Model S-611, Machine Shop, Fortelice

143   International Co., Ltd., Taiwan, China) at a resolution of 1-h (Tao et al., 2018).

144   **2.3 Lab chemical analysis and data quality assurance and control**

145   47 mm and 81 mm quartz fiber filters were measured gravimetrically for particle

146   mass concentration using a Sartorius ME 5-F electronic microbalance with a

147   sensitivity of ±1 μg (Sartorius, Göttingen, Germany) after 24 h equilibration at

148   temperature of 23±1 °C and RH of 40±5%. Microbalance was calibrated by 5 mg, 200

149   mg and 5000 mg weights before weighting. Each filter was weighed at least three

150   times before and after sampling. Differences among replicate weights were mostly

151   less than 20 μg for each sample. Net mass was obtained by subtracting pre-weight

152   from post-weight.

153   Three pieces of 0.526 cm^2 punches from each 47 mm quartz filter samples and

154   one-fourth of each 81 mm quartz filter samples were used to determine water-soluble

155   inorganic ions. The extraction of water-soluble species from each filter was put into a

156   separate 4 mL bottle, followed by 4 mL distilled-deionized water (with a resistivity

157   of >18 MΩ), and then subjected to ultrasonic agitation for 1 h for complete extraction

158   of the ionic compounds. The extract solutions were filtered (0.25 μm, PTFE,

159   Whatman, USA) and stored at 4 °C in pre-cleaned tubes until analysis. Cation (Na^+,

160   NH_4^+, K^+, Mg^{2+} and Ca^{2+}) concentrations were determined by ion chromatography

161   (Dionex ICS-1600) using a CS12A column with 20 mM Methanesulfonic Acid eluent.

162   Anions (SO_4^{2-}, NO_3^-, Cl^-, and F^-) were separated on an AS19 column in ion

163   chromatography (Dionex ICS-2100), using 20 mM KOH as the eluent. A calibration

164   was performed for each analytical sequence. Procedural blank values were subtracted

Atmospheric
Chemistry
and Physics
Discussions

165 from sample concentrations. Method detection limits (MDL) of ions were within the

166 range of 0.001 to 0.002 mg L^{-1}.

167   OC and EC were analyzed using a DRI model 2001 carbon analyzer (Atmoslytic,

168 Inc., Calabasas, CA, USA). An area of 0.526 cm^2 punched from each 47mm quartz

169 filter and 1-4 dots punched from each 81mm quartz filter were analyzed for four OC

170 fractions (OC1, OC2, OC3, and OC4 at 140 °C, 280 °C, 480 °C, and 580 °C,

171 respectively, in a helium [He] atmosphere); OP (a pyrolyzed carbon fraction

172 determined when transmitted laser light attained its original intensity after oxygen [O_2]

173 was added to the analyzed atmosphere); and three EC fractions (EC1, EC2, and EC3

174 at 580 °C, 740 °C, and 840 °C, respectively, in a 2% O_2/98% He atmosphere). Here,

175 OC is operationally defined as OC1 + OC2 + OC3 + OC4 + OP and EC is defined as

176 EC1 + EC2 + EC3 – OP for 47mm samples. However, OC is operationally defined as

177 OC1 + OC2 + OC3 + OC4 and EC is defined as EC1 + EC2 + EC3 for 81mm

178 samples due to extremely low OP level. Average field blanks were subtracted from

179 each sample filter. MDLs of OC and EC were 0.41±0.2 µgC cm^{-2} and 0.03±0.2 µgC

180 cm^{-2}, respectively.

181   To obtain high quality data of the size distributions of major chemical

182 components, bulk $PM_{2.5}$ and PM_{10} samples were synchronously collected and the

183 same chemical components were analyzed. Generally, good correlations (R^2>0.90)

184 were found in the mass concentrations of the total particle and major chemical

185 components (including total carbon (TC), NO_3^- and SO_4^{2-}) between the

186 size-segregated samples (PM_{10} and $PM_{2.1}$) and the GSAPM samplers (PM_{10} and

187 $PM_{2.5}$). The regression slopes were in the range of 0.91- 1.05, suggesting good and

Atmospheric
Chemistry
and Physics
Discussions

188   acceptable data quality of the size distributions of the major chemical components

189   (Fig.S1).

190   **2.4 Data analysis methods**

191   In this work, the cut-off point 2.1 μm was chosen to separate the fine and coarse

192   mode particles for investigating the impact of aerosol size distribution on their

193   respective MSEs. Moreover, the cut sizes of <0.43 μm and 0.43 - 2.1 μm were used to

194   separate the condensation mode and droplet mode, respectively. Continuous

195   size-distribution profiles of major chemical components are needed in order to

196   accurately calculate b_{sp} using Mie theory, and are obtained from the inversion of the

197   measured mass concentration distribution in the size bins of the Anderson 8-stage air

198   samplers using the technique described by Dong et al. (2004). However, this approach

199   is not applicable for the condensation mode because there is only one size bin in this

200   mode. Thus, MMADs of this mode are used for generating the continuous size

201   distributions of all the concerned chemical species. MMADs of this mode are

202   calculated according to:

203        $D_p = (D_{p1} \times D_{p2})^{0.5}$ (1)

204   Where D_{p1} and D_{p2} represent the lower (0.10 μm, limits of detection of Anderson

205   8-stage air sampler) and upper (0.43 μm) boundaries of this size bin, respectively. To

206   improve the resolution of b_{sp}, 401 bins were used for chemical species ranging from

207   10 nm to 100 μm, with a constant ratio between the adjacent size bins, defined as

208    $\log(D_{p2}/D_{p1})=0.01$. Further increasing the number of size bins does not have any

209   significant impact on the results, e.g., the changes in b_{sp} are smaller than 1% even if

210   the above ratio of 0.01 is replaced with 0.001.

211   The ISORROPIA II model was run at the reserved mode (Fountoukis and Nenes,

212   2007) with input data of K^+, Ca^{2+}, Mg^{2+}, NH_4^+, Na^+, SO_4^{2-}, NO_3^-, Cl^-, RH (40%), and

Atmospheric
Chemistry
and Physics
Discussions

213   temperature (25°C), to estimate the size-resolved mass concentrations of NaCl,

214    $NaNO_3$, Na_2SO_4, NH_4Cl, NH_4NO_3, $(NH_4)_2SO_4$, KCl, KNO_3, K_2SO_4, $MgCl_2$,

215    $Mg(NO_3)_2$, $MgSO_4$, $CaCl_2$, $Ca(NO_3)_2$, $CaSO_4$ and H_2O.

216   **3. Results and Discussion**

217   **3.1 Size distributions of total particle mass and major chemical components**

218   **3.1.1 Total particle mass**

219   Generally, any particle size distribution can be fitted into a combination of

220   condensation, droplet and coarse modes (John et al., 1990). Continuous log-normal

221   size distributions of particle mass including the condensation, droplet and coarse

222   modes were calculated using the method described in section 2.4 and are summarized

223   in Table 2. On annual average, 10±2%, 48±7% and 42±8% of PM_{10} mass were in the

224   condensation, droplet and coarse modes, with the average MMADs of 0.21±0.00,

225   0.78±0.07 and 4.57±0.42, respectively. This result was comparable with those

226   observed by the Micro-Orifice Uniform Deposit Impactor (MOUDI) in other cities

227   (e.g. Shenzhen and Hong Kong) of the PRD region (Bian et al., 2014; Lan et al., 2011;

228   Yu et al., 2010).

229   The estimated annual $PM_{2.5}$ concentration based on the continuous log-normal

230   size distribution was 36.4±13.2 µg m^{-3}, which was close to the synchronously

231   measured $PM_{2.5}$ (36.8±15.3 µg m^{-3}), although slightly higher than the sum of the mass

232   concentrations (34.9±13.8 µg m^{-3}) in the condensation and droplet modes. Thus, the

233   fine (sum of condensation and droplet) mode particles can reasonably represent $PM_{2.5}$.

234   Seasonal average particle mass concentrations were evidently lower in summer than

235   in the other seasons for all the three modes, were close during the other seasons for

236   the condensation and droplet modes, and were slightly higher in autumn and spring

237   than winter for the coarse mode. These results agree with the seasonal variations of

Atmospheric
Chemistry
and Physics
Discussions

238     $PM_{2.5}$ observed at the same site in 2009-2010 (Tao et al., 2014b).

239

240   *Insert Table 2*

241

242   **3.1.2 Water-soluble inorganic ions**

243   Generally, SO_4^{2-}, NO_3^- and NH_4^+ are the dominant WSIIs, especially in the

244   condensation and droplet modes. They are mainly formed through aqueous-phase

245   reactions in moisture conditions in the PRD region (Lan et al., 2011; Yu et al., 2010).

246   As expected, 77±6% SO_4^{2-}, 46±16% NO_3^- and 89±7% NH_4^+ mass concentrations were

247   in the droplet mode on annual average (Table 2). Much lower fractions for NO_3^- than

248   SO_4^{2-} and NH_4^+ in the droplet mode were mostly due to the high volatility of NH_4NO_3

249   (Zhang et al., 2008). The MMADs of the three ions in the droplet mode were in the

250   range of 0.70-0.94 μm, comparable with MOUDI measurements (0.78-1.03 μm)

251   conducted in the PRD region (Bian et al., 2014; Lan et al., 2011; Yu et al., 2010).

252   Small fractions of SO_4^{2-}, NO_3^- and NH_4^+ masses were distributed in the

253   condensation mode, e.g., 12±4%, 10±4% and 6±5%, respectively, on annual average.

254   The mass fractions of SO_4^{2-} in the condensation mode shown above were much lower

255   than those (24-29%) observed in urban Guangzhou in 2006-2007 (Yu et al., 2010),

256   suggesting gas-phase chemical reactions of SO_2 has become less important in the

257   formation of SO_4^{2-}, likely due to the dramatic reduction of SO_2 emissions in urban or

258   suburban Guangzhou in the recent decade (Zheng et al., 2009; Zheng et al., 2018).

259   Note that the MMAD in the condensation mode was 0.21 μm in Yu et al. (2010), a

260   value that is comparable with those (0.23-0.42 μm) measured using MOUDI at urban

261   sites in the PRD region (Bian et al., 2014; Lan et al., 2011; Yu et al., 2010).

262   11±5% SO_4^{2-}, 44±18% NO_3^- and 5±4% NH_4^+ mass concentrations were

263　distributed in the coarse mode. In general, NO_3^- mainly exists in the form of NH_4NO_3

264　in the condensation and droplet modes and associates with base cations in the coarse

265　mode (e.g., $Ca(NO_3)_2$ and $NaNO_3$) (Zhang et al., 2015a). More than 50% NO_3^- mass

266　concentrations were distributed in the coarse mode in summer and autumn when

267　ambient temperatures were high. The MMADs of NO_3^- in the coarse mode were

268　4.15 ± 0.52 and 4.36 ± 0.31 μm in summer and autumn, respectively, slightly lower than

269　those of Ca^{2+} (4.10 ± 0.42 and 4.72 ± 0.47 μm in the same seasons), but evidently higher

270　than those of Na^+ (3.60 ± 0.19 and 3.64 ± 0.27 μm) (Table 2). This suggests that

271　NH_4NO_3 was prone to dissociate to $HNO_{3(g)}$ in summer and autumn due to the high

272　ambient temperatures with released $HNO_{3(g)}$ further reacting with mineral dust and to

273　a less extent with sea salt particles. In comparison, the MMADs of SO_4^{2-} in the coarse

274　mode were in between of those of Ca^{2+} and Na^+, likely due to uptake of $H_2SO_{4(g)}$ by

275　both mineral dust and sea salt particles (Zhang et al., 2015a). In contrast, the MMAD

276　of NH_4^+ in the coarse mode was 3.25 ± 0.69 μm, much smaller than those of SO_4^{2-} and

277　NO_3^-, suggesting that NH_4^+ in the coarse mode was likely from hygroscopic growth of

278　NH_4^+ in the droplet mode (Tian et al., 2014a).

279　　It is also worth mentioning that most of Cl^- was distributed in the coarse mode

280　and its MMAD (3.77 ± 0.35 μm) was very close to that of Na^+ (3.75 ± 0.38 μm),

281　especially in summer when air masses were originated from the China South Sea (Tao

282　et al., 2017b; Xia et al., 2017). The mole ratios of Cl^-/Na^+ were less than 1.0 in all the

283　seasons but spring due to the reactions between sea salt and acid gasses ($HNO_{3(g)}$ and

284　$H_2SO_{4(g)}$) (Zhuang et al., 1999a). The excess Cl^- in the coarse mode in spring was

285　likely due to the aged biomass burning particles from the southeast Asian. In fact, the

286　concentration of the typical biomass burning tracer K^+ in the coarse mode was higher

287　in spring than in the other seasons (Zhang et al., 2015c). In any case, sea salt was

Atmospheric
Chemistry
and Physics
Discussions

288   mainly distributed in the coarse mode rather than the droplet mode in urban

289   Guangzhou.

3.1.3 OC and EC

291   OC and EC in fine particles can be produced from both primary emissions of

292   vehicle exhaust, coal combustion, biomass burning and secondary formation (Chow et

293   al., 2011; Gentner et al., 2012; Gentner et al., 2017; Hallquist et al., 2009; Zheng et al.,

294   2006). In general, fresh OC and EC particles emitted from vehicle exhaust, coal

295   combustion and biomass burning should be distributed in the condensation mode

296   (Schwarz et al., 2008; Zhang et al., 2012b). Only 13±4% of OC and 31±7% of EC

297   mass concentrations were distributed in the condensation mode in the present study

298   (Table 2). OC/EC ratios were in the range of 0.9-1.6 in the condensation mode,

299   suggesting that vehicle exhaust was the dominant source of OC and EC in this particle

300   size range (Huang et al., 2006a; Schwarz et al., 2008; Shiraiwa et al., 2007; Watson et

301   al., 2001; Wu et al., 2017). 62±9% of OC and 55±7% of EC mass concentrations were

302   distributed in the droplet mode (Table 2), similar to that of SO_4^{2-}. These numbers were

303   similar to those observed in the other cities of the PRD region, and was previously

304   identified to be mainly caused by in-cloud aerosol processing (Huang et al., 2006b).

305   Cloud processing indeed plays important roles in forming droplet mode aerosols in

306   urban Guangzhou (Tao et al., 2018). OC/EC ratios were in the range of 2.2-3.2 in the

307   droplet mode, much higher than those in the condensation mode, suggesting that OC

308   in the droplet mode was mainly aged or secondary particles (Day et al., 2015; Huang

309   et al., 2006a; Wu and Yu, 2016).

310   Although only one size bin was available in the condensation mode in this study,

311   the estimated MMADs of OC and EC in this mode were comparable with those

312   (0.25-0.34 μm) measured using MOUDI with 3 bins in this size range at suburban

Atmospheric
Chemistry
and Physics
Discussions

313   sites (e.g. Hong Kong and Shenzhen) (Lan et al., 2011; Yu et al., 2010). The MMADs

314   of OC and EC in the droplet mode were 0.76±0.07 μm and 0.66±0.08 μm,

315   respectively, which were slightly lower than those (0.7-1.0 μm for OC and 0.8-1.0 μm

316   for EC) found in earlier studies in the PRD region (e.g. Guangzhou, Hong Kong and

317   Shenzhen) (Lan et al., 2011; Yu et al., 2010). Noticeably, the MMADs of OC and EC

318   in the droplet mode were very close to those (0.73 μm for OC and 0.77 μm for EC)

319   measured in summer at a suburban site of Hong Kong, where the loadings of the

320   dominant chemical components (e.g. OC, EC and SO_4^{2-}) were low (Yu et al., 2010).

321   Road dust and biogenic aerosols were generally considered as the major sources

322   of OC and EC in the coarse mode (Ho et al., 2003; Zhang et al., 2015b). Significant

323   fractions of OC (25±8%) and EC (14±7%) mass concentrations were distributed in the

324   coarse mode. These numbers were comparable with those (13-38% for OC and 4-16%

325   for EC) measured at suburban sites of Guangzhou, Shenzhen and Hong Kong (Lan et

326   al., 2011; Yu et al., 2010), but were lower than those (51-57% for OC and 17-21% for

327   EC) measured in urban Guangzhou in 2006-2007. The MMADs of OC (3.73±0.58 μm)

328   and EC (3.69±0.65 μm) in the coarse mode were close to those (3.8-4.3 μm for OC

329   and 3.7-4.1 μm for EC) measured in suburban of Hong Kong, although smaller than

330   those (4.8-5.2 μm for OC and 5.0-5.2 μm for EC) measured in suburban of Shenzhen

331   and urban of Guangzhou (Lan et al., 2011; Yu et al., 2010). These results suggested

332   that the MMADs of OC and EC might decrease with their decreasing coarse mode

333   mass fractions. Annual PM_{10} concentrations in 2015-2016 in this study were 40%

334   lower than those in 2006-2007 in the PRD region, which further supported the above

335   hypothesis (Yu et al., 2010).

3.2 Closures of particle mass and number concentrations and b_{sp}

3.2.1 Closure of particle mass concentration

To investigate the impact of chemical species in different size modes on b_{sp}, particle mass concentrations in the different modes were first reconstructed based on mass concentrations of individual known chemical components. The dominant water-soluble inorganic species including $NaCl$, $NaNO_3$, Na_2SO_4, NH_4NO_3, $(NH_4)_2SO_4$, K_2SO_4, $CaSO_4$ and $Ca(NO_3)_2$ were determined using the ISORROPIA II thermodynamic equilibrium model as mentioned in section 2.4. A ratio of OM to OC of 1.4, 1.6 and 1.6 would be appropriate for the condensation, droplet and coarse mode, respectively, which was based on the findings of a previous study that suggested an average OM/OC ratio of 1.57 and a range of 1.4-1.8 in an urban environment of the PRD region (He et al., 2011). In our previous study (Tao et al., 2017b), mass concentration of crustal element oxides in $PM_{2.5}$ was estimated from the measurements of five crustal elements (Al, Si, Ca, Fe and Ti) in urban Guangzhou. This approach cannot be used in the present study due to the lack of crustal elements measurements. Alternatively, crustal element oxides mass concentration was estimated from Ca^{2+} mass concentration because of their good correlations as was found in our previous study (Fig. S2) (Tao et al., 2017b). Moreover, source profiles of soil dust (representing crustal element oxides) in cities of southern China also suggested that Ca^{2+} accounted for 5% of total soil dust in $PM_{2.5}$ (Sun et al., 2019). On annual average, the estimated crustal element oxides accounted for 8±2%, 10±4% and 29±5% of the total particle mass concentrations in the condensation, droplet and coarse mode, respectively. The reconstructed mass concentrations accounted for 79±3%, 82±6% and 57±6% of the total in the condensation, droplet and coarse mode, respectively.

Atmospheric
Chemistry
and Physics
Discussions

361   As shown in Fig. 2, OM, EC, $(NH_4)_2SO_4$, NH_4NO_3 and crustal element oxides

362   dominated in different modes in four seasons. For example, OM and EC accounted

363   for 31-39% and 14-19%, respectively, of particle mass in the condensation mode, OM,

364    $(NH_4)_2SO_4$, crustal element oxides and NH_4NO_3 accounted for 19-34%, 18-22%, 6-15%

365   and 4-11%, respectively, in the droplet mode, and crustal element oxides, OM and

366    $CaSO_4$ accounted for 22-34%, 12-17% and 4-5%, respectively, in the coarse mode. In

367   addition, the total of the other identified chemical species only accounted for less than

368   10% of the total particle mass in every mode. For example, Na_2SO_4 and K_2SO_4

369   mainly distributed in the droplet mode and together they accounted for only 2-5% of

370   the particle mass in this mode. $NaCl$, $NaNO_3$ and $Ca(NO_3)_2$ mainly distributed in the

371   coarse mode and each of these species accounted for less than 2% of the total particle

372   mass in this mode.

373

374   *Insert Figure 2*

375

376   **3.2.2 Closure of particle number concentration**

377   To estimate the contribution of individual chemical species on b_{sp} using Mie

378   theory, number size distributions of the dominant chemical species were needed and

379   were calculated according to the method described in Lin et al. (2014). As shown in

380   Fig. 3, most chemical species (except $(NH_4)_2SO_4$ in summer) had much higher

381   number concentrations in the condensation than droplet or coarse mode. Although the

382   estimated number median aerodynamic diameters (NMADs) of the number

383   concentrations of individual chemical species mainly distributed in the range of

384   100-120 nm, the estimated NMADs of particle number concentrations were always

385   close to about 100 nm in four seasons. This was because the estimated MMADs of

386   particle mass concentrations were a constant value (0.21 μm) based on only one bin in

387   the condensation mode. Moreover, average densities of particle in the condensation

388   mode only changed a little in four seasons because OM and EC were always the

389   dominant chemical species in this mode.

390   In contrast, the NMADs of particle number concentrations simultaneously

391   measured by the SMPS and APS distributed in the range of 40-80 nm (Fig. 4), which

392   shifted to smaller sizes than those estimated from the size-segregated chemical

393   species mass concentrations. This was because SMPS and APS collected dried

394   particles while the size-segregated sampler collected ambient particles. D_g of particles

395   measured by SMPS can be converted to D_a using the average particle density

396   calculated from the synchronously measured size-segregated individual chemical

397   species mass concentrations and densities. In any case, the NMADs of particle

398   number concentrations were less than 100 nm regardless of using SMPS and APS

399   measurements or the estimated size-segregated chemical species mass concentrations.

400   As shown in Fig. 3 and Fig. 4, most of particle numbers were in the range of 10 -

401   400 nm either observed by the SMPS or estimated from the size-segregated chemical

402   species mass concentrations. Total particle number concentration in the range of 10

403   nm-10 μm measured by the SMPS and APS were 7038±2250 cm^{-3}, 9774±1471 cm^{-3},

404   5694±1942 cm^{-3} and 10801±2986 cm^{-3}, respectively, in spring, summer, autumn and

405   winter, which were 1.09±0.24, 2.66±0.48, 1.05±0.20 and 2.33±0.67 times of those

406   estimated by the size-segregated chemical species mass concentrations.

407   NMADs estimated from the size-segregated chemical species mass

408   concentrations were close to those measured by the SMPS and APS in spring and

409   autumn, resulting in the close estimation of particle number concentrations to the

410   measured ones. In contrast, the estimated particle number concentrations from the the

411 size-segregated chemical species mass concentrations were evidently lower than those

412 measured by the SMPS and APS in summer and winter, due to the much higher

413 NMADs (100 nm) estimated from the size-segregated chemical species mass

414 concentrations than those (about 30 or 40 nm) measured by the SMPS and APS.

415 Fortunately, the single particle scattering efficiencies of chemical species in the

416 condensation mode at the wavelength 520 nm were much lower than those in the

417 droplet mode and the coarse mode (Fig S3).

418   To exclude the large uncertainties in the estimated particle number concentration

419 caused by condensation mode particles (which were due to the design flaws of

420 size-segregated sampler), particles smaller than 430 nm were not included in the

421 calculation below. The estimated particle number concentrations in the range of 430

422 nm-10 μm based on the size-segregated chemical species mass concentrations were

423 only slightly higher than those measured by the SMPS and APS. This was likely

424 because particles in the droplet mode may shift to the smaller sizes (<430 nm) during

425 the dry process by Nafion tube. Moreover, most of EC particles in the droplet mode

426 were internally mixed with OM or inorganic salts in the real world, which also may

427 result in overestimating the particle number concentrations by the size-segregated

428 chemical species mass concentrations (Wu et al., 2016; Yu et al., 2010). Correlation

429 coefficients between the estimated and measured particle number concentrations in

430 the range of 430 nm-10 μm were significantly improved when the intercepts in the

431 linear regression equations were retained. To some extent, the intercepts represented

432 the measurement or estimation errors of SMPS and APS and models. In any case,

433 good correlations (R^2>0.81) between the estimated daily particle number

434 concentrations and the measured ones were found and the slopes ranged from 0.79 to

435 1.03 in the four seasons (Fig. 5). These results suggested that the estimated particle

436   number concentrations were acceptable in the range of 430 nm-10 μm, noting that

437   particles in this size range dominate particle scattering efficiency.

438

439   *Insert Figure 3*

440   *Insert Figure 4*

441   *Insert Figure 5*

442

443

444   **3.2.3 Closure between the measured and estimated b$_{sp}$**

445   Although the number concentrations in the condensation mode were

446   underestimated, good correlations ($R^2 > 0.92$) were found between the measured and

447   estimated b$_{sp}$ with the slopes being 0.87, 0.87, 0.85 and 0.89 in spring, summer,

448   autumn and winter, respectively (Fig 6). On annual arithmetic average, the estimated

449   b$_{sp}$ can explain 91±10% of the measured b$_{sp}$. The residual fractions were likely related

450   to the chosen convert factor between OM and OC, measurements and sampling errors

451   of chemical species (especially NO_3^-), errors from the models (ISORROPIA II model,

452   Mie model, and especially the inversion technique method), and measurement errors

453   caused by the size-segregated sampler (Vaughan, 1989). Magnitudes of the

454   uncertainties caused by these sources are discussed below.

455   Although the convert factor of 1.6 between OM and OC was reasonable in urban

456   environment, a value of as high as 1.8 was found in literature (He et al., 2011). In

457   addition, OC mass concentrations were likely underestimated due to the OC/EC

458   protocol for size-segregated samples. Nevertheless, the estimated b$_{sp}$ can only be

459   increased by less than 3% if increasing the convert factor to 1.8 in the droplet mode.

460   Note that a previous study at the Fresno Supersite increased the estimated b$_{sp}$ by about

Atmospheric
Chemistry
and Physics
Discussions

461   10% when increasing the convert factor from 1.4 to 1.8, likely due to the high mass

462   fraction of OC in fine particle at this site (Watson et al., 2008).

463   Different from the other chemical species, NH_4NO_3 can dissociate into $HNO_{3(g)}$

464   and $NH_{3(g)}$ during the filter gravimetric weighing process under dry condition. To

465   evaluate the evaporative loss of NH_4NO_3, synchronous online data of NO_3^- were also

466   measured by an In-situ Gas and Aerosol Composition monitoring system at hourly

467   temporal resolution (Fig. S4). Seasonal average NO_3^- concentrations were 42%

468   ($PM_{2.5}$), 39% (PM_{10}), 42% ($PM_{2.5}$) and 19% ($PM_{2.5}$) less from filter measurements

469   than online measurements in spring, summer, autumn and winter, respectively.

470   Adjusting the filter NO_3^- data using the above ratios can increase the estimated b_{sp} by

471   7%, 2%, 4% and 2% in the respective season.

472

473   *Insert Figure 6*

474

475   Meanwhile, the measured b_{sp} could also be underestimated due to the

476   dissociation of NH_4NO_3 during the dry processes of ambient particles through the

477   Nafion dryer. A previous study indicated the measured b_{sp} being decreased by less

478   than 10% due to the dissociation of NH_4NO_3 in a heated nephelometer (Bergin et al.,

479   1997). In the present study, the chamber temperatures of nephelometer were less

480   than 300 K and the particle residence time in both the Nafion dryer and the

481   nephelometer chamber was about 7 seconds. Thus, the bias in the measured b_{sp}

482   should be less than 2% in any season according to the relationship among the loss

483   of b_{sp}, residence time and the temperature in chamber in a previous study (Bergin et

484   al., 1997). Combining all of the above-mentioned factors, the adjusted estimated b_{sp}

485   would increase to the level of 92%, 87%, 87% and 89% of the measured b_{sp} in

486   spring, summer, autumn and winter, respectively. This means the above methods for

487   estimating b_{sp} were reasonable with the adjusted estimated values explaining 87-92%

488   of the measured values after the filter-based NO_3^- concentrations were adjusted

489   based on the online data. Thus, the errors from the models and size-segregated

490   samplers may account for remaining 8-13% of the measured b_{sp}.

491   Generally, the estimated seasonal average b_{sp} were 146 ± 40 Mm^{-1}, 99 ± 33 Mm^{-1},

492   169 ± 54 Mm^{-1} and 151 ± 71 Mm^{-1} in spring, summer, autumn and winter,

493   respectively (Fig. 7). The particles in the condensation, droplet and coarse modes

494   contributed 6-7%, 81-86% and 8-12%, respectively, to the estimated b_{sp}. OM and

495   EC were the dominant contributors, accounting for 32-41% and 30-37%,

496   respectively, of the estimated b_{sp} in the condensation mode. OM and secondary

497   inorganic aerosols (sum of $(NH_4)_2SO_4$ and NH_4NO_3) were the dominant

498   contributors, accounting for 27-44% and 27-34%, respectively, of the estimated b_{sp}

499   in the droplet mode. Unidentified fraction, crustal element oxides and OM were the

500   dominant contributors, accounting for 26-47%, 16-29% and 19-27%, respectively,

501   of the estimated b_{sp} in the coarse mode. The sum of the dominant contributors,

502   including OM, EC, secondary inorganic aerosols and crustal element oxides,

503   accounted for 70-79% of the estimated b_{sp} in the four seasons. In contrast, the sum

504   of the other chemical species (including NaCl, $NaNO_3$, Na_2SO_4, K_2SO_4, $CaSO_4$,

505    $Ca(NO_3)_2$, H_2O) accounted for 5-10% and the unidentified fraction, 12-23% of the

506   estimated b_{sp}. In conclusion, visibility degradation was determined by the dominant

507   chemical species (e.g. OM, EC, secondary inorganic aerosols and crustal element

508   oxides) in the fine mode (both condensation and droplet), which agreed with the

509   results of the original and revised IMPORVE formulas (Pitchford et al., 2007).

510

Atmospheric
Chemistry
and Physics
Discussions

511   *Insert Figure 7*

512

3.3 Key factors for variations of particle and chemical species MSEs

3.3.1 The estimated MSEs of particle and chemical species

515   To conveniently explore the control factors of particle MSE, the dominant

516   chemical species' MSEs were estimated by their mass concentrations and the

517   estimated b_{sp}, according to the measured chemical species mass concentrations in

518   section 3.1 and the estimated b_{sp} in section 3.2. Here, only the MSEs of particle,

519    $(NH_4)_2SO_4$, NH_4NO_3, OM, EC, crustal element oxides and unidentified fraction in the

520   condensation, droplet, coarse, and fine modes (sum of condensation and droplet

521   modes) were estimated (Table 3), considering these chemical species accounted for

522   more than 90% of the estimated b_{sp}. Moreover, an external mixing of individual

523   chemical species was assumed in the estimation.

524

525   *Insert Table 3*

526

527   Undoubtedly, the particle MSE should be underestimated because the estimated

528   b_{sp} was 11-15% less of the measured b_{sp} in four seasons, as discussed in section 3.2.

529   The measured b_{sp} would be biased low by about 3% due to the evaporation of

530   NH_4NO_3, while the NO_3^- mass concentrations based the filter measurements were

531   biased low by 5%, 3%, 9% and 6% in spring, summer, autumn and winter,

532   respectively. Thus, the MSEs of NO_3^- would be underestimated by 9%, 13%, 6% and

533   5% in the respective season in the real world. In conclusion, the MSEs of particle and

534   chemical species were underestimated by less than 13%.

535   On annual average, the estimated particle MSEs in the condensation, droplet and

536 coarse modes were 2.1±0.2 m^2 g^{-1}, 4.3±0.2 m^2 g^{-1} and 0.5±0.0 m^2 g^{-1}, respectively.

537 The estimated particle MSE in the fine mode (sum of condensation and droplet modes,

538 similar to PM$_{2.5}$) was 3.7±0.2 m^2 g^{-1}, which was slightly higher than the value of 3.5

539 m^2 g^{-1} estimated in 2009-2010 in urban Guangzhou (Tao et al., 2014b). Seasonal

540 variations of the estimated MSEs in the fine mode followed the sequence of winter

541 (3.9±0.2 m^2 g^{-1}) > autumn (3.8±0.2 m^2 g^{-1}) > summer (3.6±0.2 m^2 g^{-1}) > spring

542 (3.5±0.1 m^2 g^{-1}). Evidently, the estimated MSEs in the fine mode were slightly higher

543 in autumn and winter than spring and summer, which also agreed with the previous

544 studies in urban Guangzhou (Andreae et al., 2008; Jung et al., 2009a).

545 On annual average, the estimated MSEs of (NH$_4$)$_2$SO$_4$, NH$_4$NO$_3$, OM and crustal

546 element oxides (equal to fine soil in the IMPROVE formulas) in the fine mode were

547 4.4±0.8, 4.5±1.5, 4.6±0.3 and 2.6±0.1 m^2 g^{-1}, respectively, which were higher than

548 those (3.0, 3.0, 4.0 and 1.0 m^2 g^{-1}, respectively) from using the original IMPROVE

549 formula (Hand and Malm, 2007; Malm and Hand, 2007; Pitchford et al., 2007). As

550 shown in Table 3, the MSEs of (NH$_4$)$_2$SO$_4$, NH$_4$NO$_3$, OM and crustal element oxides

551 in the fine mode depended on their mass fractions in the droplet mode with high

552 MSEs. In the original IMPROVE formula, MSEs of these chemical species were

553 estimated using the multiple linear regression model according to the chemical

554 components in PM$_{2.5}$ and b$_{sp}$ from IMPROVE network, noting that significant mass

555 fractions of particle were in the condensation mode at the regional sites of IMPROVE

556 network and an urban site in U.S.A. (Cabada et al., 2004; Hand et al., 2002; Malm et

557 al., 2003). In contrast, in the present study most mass fractions of the dominant

558 chemical species (e.g. (NH$_4$)$_2$SO$_4$, NH$_4$NO$_3$ and OM) in the fine mode were

559 distributed in the droplet rather than condensation mode. These results suggested the

560 higher MSEs of (NH$_4$)$_2$SO$_4$, NH$_4$NO$_3$ and OM in the fine mode in this study were

561   likely due to their significant mass fractions in the droplet mode. In fact, the MSE of

562   fine soil in the IMPROVE formulas would represent the MSE of the bulk mode rather

563   than the fine mode (Hand and Malm, 2007). The average MSEs of the bulk mode was

564   1.0 ± 0.2 m^2 g^{-1} in this study, which was similar to that in the IMPROVE formulas.

565   On annual average, the estimated MSEs of $(NH_4)_2SO_4$, NH_4NO_3 and OM were

566   4.7 ± 0.6, 4.8 ± 0.9 and 5.3 ± 0.2 m^2 g^{-1} in the droplet mode, and were 2.1 ± 0.5, 2.3 ± 0.8

567   and 2.7 ± 0.1 m^2 g^{-1} in the condensation mode, respectively, which were lower than

568   those in the large mode (similar to droplet mode) and were slightly lower than those

569   in the small mode (similar to condensation mode) in the revised IMPROVE formula

570   (Pitchford et al., 2007). Theoretically, the highest MSEs of $(NH_4)_2SO_4$, NH_4NO_3 and

571   OM would be found in about 0.55 µm in mass median geometric diameters (MMGD)

572   at the wavelength 550 nm according to Mie theory. However, the MMADs of

573     $(NH_4)_2SO_4$, NH_4NO_3 and OM were 0.76 - 0.80 µm (equal to about 0.60-0.64 µm in

574   MMGD) in the droplet mode and were 0.21 µm (equal to about 0.16-0.18 µm in

575   MMGD) in the condensation mode in this study, which were larger than 0.50 µm in

576   MMGD in the large mode and were lower than 0.20 µm in MMGD in the small mode

577   in the revised IMPROVE formula. Thus, the higher MMGDs in the droplet mode and

578   the lower MMGDs of $(NH_4)_2SO_4$, NH_4NO_3 and OM in the condensation mode in this

579   study maybe result in their lower MSEs compared with those in the revised

580   IMPROVE formula. In addition, the underestimated b_{sp} would also result in

581   underestimating their MSEs in the condensation and droplet modes in this study.

582   Although the contribution of EC to b_{sp} was not considered in the IMPROVE

583   formulas, its mass extinction efficiency (10 m^2 g^{-1}) considered both scattering and

584   absorption abilities (Hand and Malm, 2007). In fact, the theoretical average mass

585   absorption efficiency (MAE) of EC in fine particle was 7.5 m^2 g^{-1} at the wavelength

Atmospheric
Chemistry
and Physics
Discussions

586   550 nm (Wu et al., 2016). Thus, mass extinction efficiency of EC was also about 10

587     $m^2 \ g^{-1}$ in this study, suggesting the estimated EC MSEs were comparable with the

588   IMPROVE formulas. The estimated MSEs of coarse particle was $0.5 \pm 0.0 \ m^2 \ g^{-1}$,

589   which was also comparable with the value of $0.6 \ m^2 \ g^{-1}$ in the IMPROVE formulas.

590   Noticeably, sea salt was mainly distributed in the coarse mode rather than droplet

591   mode in this study. In addition, the unidentified fraction with large mass fraction and

592   the high MSE in the fine mode was not considered in the IMPROVE formulas,

593   although it accounted for a significant contribution of the estimated b_{sp} in this study

594   (Fig. 7). In conclusion, EC and unidentified fraction rather than sea salt should be

595   considered in estimating b_{sp}, especially when EC and unidentified fraction accounted

596   for significant mass fractions of fine particles.

597   **3.3.2 Impact of size distribution on particle and chemical species MSE**

598   As discussed in section 3.3.1, seasonal average MSEs in the coarse mode

599   fluctuated in a small range of 0.4-0.5 $m^2 \ g^{-1}$, while those in the fine mode in a slightly

600   larger range of 3.5-3.9 $m^2 \ g^{-1}$, but the percentage changes are in similar magnitudes

601   (10-20%). Only variations of fine particle MSE were discussed below as an example.

602   It is worth to mention that fine particle MSE increased with its mass concentrations in

603   IMPROVE network (Lowenthal and Kumar, 2004), but such a phenomenon was not

604   founded in the present study. As shown in Fig. 8, the seasonal variations of fine

605   particle MSE were mainly caused by particle fractions in the size range of 0.4-0.9 μm,

606   which belong to the droplet mode. In this mode, the MSEs of $(NH_4)_2SO_4$ and NH_4NO_3

607   and OM were higher while those of the other chemical species were lower than the

608   overall particle MSE. Note that the overall particle MSE depends on the mass

609   concentrations and MSEs of individual chemical components. Thus, the seasonal

Atmospheric
Chemistry
and Physics
Discussions

610   average MSEs of fine particle were dominated by the seasonal average mass fractions

611   and associated MSEs of $(NH_4)_2SO_4$ and NH_4NO_3 and OM in the droplet mode.

612

613   *Insert Figure 8*

614

615   The sum of the products of seasonal average mass concentration and MSEs of

616   the above three chemical species in the droplet mode was 1.8, 2.1, 2.3 and 2.5 m^2 g^{-1}

617   in spring, summer, autumn and winter, respectively. As expected, the seasonal

618   variations of fine particle MSE followed the sequences of winter (3.9 ± 0.2 m^2 g^{-1}) >

619   autumn (3.8 ± 0.2 m^2 g^{-1}) > summer (3.6 ± 0.2 m^2 g^{-1}) > spring (3.5 ± 0.1 m^2 g^{-1}).

620   Noticeably, fine particle MSE was determined by the average MSEs of the dominant

621   chemical species, rather than their mass fractions which were much smaller than 1.0.

622   Different from the approach used for fine particle MSE, the MSEs of $(NH_4)_2SO_4$,

623   NH_4NO_3 and OM in the droplet mode were determined using measurement-based

624   their mass size distributions prescribed as log-normal size distributions. The three

625   parameters describing the log-normal size distributions include mass concentration (in

626   the range of 0.43 - 2.1 μm), MMAD and standard deviation (σ). Thus, the MSEs of

627     $(NH_4)_2SO_4$, NH_4NO_3 and OM should depend on their MMADs and σ values. Seasonal

628   average σ values of $(NH_4)_2SO_4$, NH_4NO_3 and OM were in the range of 0.18-0.21,

629   0.18-0.21 and 0.22-0.26, respectively, while the corresponding MMADs in the range

630   of 0.72-0.92, 0.75-0.90 and 0.73-0.78 μm, respectively (Fig. 9). Generally, the

631   seasonal average MSEs of $(NH_4)_2SO_4$, NH_4NO_3 and OM in the droplet mode were

632 higher with the lower σ values (or MMADs) when MMADs (σ values) were close.

633 However, the MSE of OM in summer was 5.2 $m^2 g^{-1}$, which was lower than 5.3 $m^2 g^{-1}$

634 in autumn, although σ values and MMADs in summer were lower than those in

635 autumn. This was mainly related with the evident fluctuation the MSE of OM in the

636 range of 0.6-0.7 μm.

637

638 *Insert Figure 9*

639

640 In conclusion, the fine particle MSE was determined by the sum of the products

641 of average mass fractions and MSEs of $(NH_4)_2SO_4$ and NH_4NO_3 and OM in the

642 droplet mode. The MSEs of the above three chemical species in the droplet mode

643 depended on both their σ value and MMADs. Generally, fine particle MSE mainly

644 related with OM due to its high mass and MSE in the droplet mode in urban

645 Guangzhou.

646 **4. Summary and implication**

647 Size- and chemically-resolved particle number and mass concentration were

648 measured in urban Guangzhou in different seasons during 2015-2016 and the data

649 were used to estimate particle MSE. SO_4^{2-} and NH_4^+ mainly distributed in the droplet

650 mode, EC in both condensation and droplet modes, and bulk particle, NO_3^-, OC, Na^+,

651 Ca^{2+} and Cl^- in both droplet and coarse modes. The estimated b_{sp} can represent 85-89%

652 of the measured b_{sp} based on the size-segregated chemical compositions according to

653 ISORROPIA II thermodynamic equilibrium model and Mie theory model. The largest

Atmospheric
Chemistry
and Physics
Discussions

Open Access

654   contributors to b_{sp} were the chemical species in the droplet mode with the highest

655   MSEs.

656   MSEs of the dominant chemical species were noticeably different in this study

657   than those in the original and revised IMPROVE formulas. The MSEs of $(NH_4)_2SO_4$,

658   NH_4NO_3 and OM in the fine mode were higher than those in the original IMPROVE

659   formula, and in the droplet mode were lower than those in the revised IMPROVE

660   formula. In any case, b_{sp} would be underestimated in urban Guangzhou using the

661   original or revised IMPROVE formulas because the unidentified chemical species

662   (and associated mass fractions) in the droplet mode accounted for a large fraction of

663   b_{sp} and this portion was not included in these formulas. Moreover, MSEs of chemical

664   species would be overestimated in the original and revised IMPROVE formulas using

665   multiple linear regression model when the unidentified species was ignored. In

666   addition, sea salt was found in the coarse mode in this study, differing from the set up

667   in the IMPROVE formulas which is in the droplet mode. It can be concluded that the

668   estimated b_{sp} in Guangzhou based on the revised IMPROVE formula would have

669   large biases, even though good correlations between estimated and measured b_{sp} was

670   found.

671   MSEs of fine particles are controlled by the relative mass fractions of the

672   dominant chemical components (e.g., $(NH_4)_2SO_4$, NH_4NO_3 and OM) and associated

673   size distributions (e.g. σ and MMAD). Localized b_{sp} formulas are thus needed for

674   better estimating particle MSE because particle size distributions of individual

675   chemical species vary significantly in space and time.

676 *Data availability. Data used in this study are available from Jun Tao (taojun@scies.org).*

677 *Competing interests. The authors declare that they have no conflict of interest.*

678

679 **Acknowledgments**

683 **References**

684 Andreae, M. O., Schmid, O., Yang, H., Chand, D., Zhen Yu, J., Zeng, L.-M., and Zhang, Y.-H.: Optical
685   properties and chemical composition of the atmospheric aerosol in urban Guangzhou, China,
686   Atmospheric Environment, 42, 6335-6350, 2008.

687 Bergin, M. H., Ogren, J. A., Schwartz, S. E., and McInnes, L. M.: Evaporation of Ammonium Nitrate
688   Aerosol in a Heated Nephelometer: Implications for Field Measurements, Environmental Science
689   & Technology, 31, 2878-2883, 10.1021/es970089h, 1997.

690 Bian, Q., Huang, X. H., and Yu, J. Z.: One-year observations of size distribution characteristics of
691   major aerosol constituents at a coastal receptor site in Hong Kong – Part 1: Inorganic ions and
692   oxalate, Atmospheric Chemistry and Physics, 14, 9013-9027, 2014.

693 Cabada, J. C., Rees, S., Takahama, S., Khlystov, A., Pandis, S. N., Davidson, C. I., and Robinson, A. L.:
694   Mass size distributions and size resolved chemical composition of fine particulate matter at the
695   Pittsburgh supersite, Atmospheric Environment, 38, 3127-3141, 2004.

696 Cao, J., Wang, Q., Chow, J. C., Watson, J. G., Tie, X., Shen, Z., Wang, P., and An, Z.: Impacts of
697   aerosol compositions on visibility impairment in Xi'an, China, Atmospheric Environment, 59,
698   559-566, 2012.

699 Chen, P., Wang, T., Lu, X., Yu, Y., Kasoar, M., Xie, M., and Zhuang, B.: Source apportionment of
700   size-fractionated particles during the 2013 Asian Youth Games and the 2014 Youth Olympic
701   Games in Nanjing, China, Science of The Total Environment, 579, 860-870, 2017.

702 Cheng, Y., Wiedensohler, A., Eichler, H., Su, H., Gnauk, T., Brüggemann, E., Herrmann, H.,
703   Heintzenberg, J., Slanina, J., and Tuch, T.: Aerosol optical properties and related chemical
704   apportionment at Xinken in Pearl River Delta of China, Atmospheric Environment, 42, 6351-6372,
705   2008.

706 Cheng, Y. F., Berghof, M., Garland, R. M., Wiedensohler, A., Wehner, B., Muller, T. J., Su, H., Zhang,
707   Y. H., Achtert, P., and Nowak, A.: Influence of soot mixing state on aerosol light absorption and
708   single scattering albedo during air mass aging at a polluted regional site in northeastern China,
709   Journal of Geophysical Research, 114, 2009.

710 Cheng, Z., Jiang, J. S., Chen, C., Gao, J., Wang, S., Watson, J. G., Wang, H., Deng, J., Wang, B., and
711   Zhou, M.: Estimation of aerosol mass scattering efficiencies under high mass loading: case study

Atmospheric
Chemistry
and Physics
Discussions

712   for the megacity of Shanghai, China, Environmental Science & Technology, 49, 831-838, 2015.

713   Chow, J. C., Watson, J. G., Lowenthal, D. H., Chen, L. W. A., and Motallebi, N.: $PM_{2.5}$ source profiles

714   for black and organic carbon emission inventories, Atmospheric Environment, 45, 5407-5414,

715   2011.

716   Day, M. C., Zhang, M., and Pandis, S. N.: Evaluation of the ability of the EC tracer method to estimate

717   secondary organic carbon, Atmospheric Environment, 112, 317-325, 2015.

718   Dong, Y., Hays, M. D., Smith, N. D., and Kinsey, J. S.: Inverting cascade impactor data for

719   size-resolved characterization of fine particulate source emissions, Journal of Aerosol Science, 35,

720   1497-1512, 2004.

721   Fountoukis, C., and Nenes, A.: ISORROPIA II: a computationally efficient thermodynamic equilibrium

722   model for $K^+–Ca^{2+}–Mg^{2+}–NH_4^+–Na^+–SO_4^{2-}−NO_3^−–Cl^−–H_2O$ aerosols, Atmospheric Chemistry

723   and Physics, 7, 4639-4659, 2007.

724   Gao, Y., Lai, S., Lee, S. C., Yau, P. S., Huang, Y., Cheng, Y., Wang, T., Xu, Z., Yuan, C., and Zhang, Y.:

725   Optical properties of size-resolved particles at a Hong Kong urban site during winter, Atmospheric

726   Research, 155, 1-12, 2015.

727   Gentner, D. R., Isaacman, G., Worton, D. R., Chan, A. W. H., Dallmann, T. R., Davis, L. E., Liu, S.,

728   Day, D. A., Russell, L. M., and Wilson, K. R.: Elucidating secondary organic aerosol from diesel

729   and gasoline vehicles through detailed characterization of organic carbon emissions, Proceedings

730   of the National Academy of Sciences of the United States of America, 109, 18318-18323, 2012.

731   Gentner, D. R., Jathar, S. H., Gordon, T. D., Bahreini, R., Day, D. A., Haddad, I. E., Hayes, P. L., Pieber,

732   S. M., Platt, S. M., and De Gouw, J. A.: Review of Urban Secondary Organic Aerosol Formation

733   from Gasoline and Diesel Motor Vehicle Emissions, Environmental Science & Technology, 51,

734   1074-1093, 2017.

735   Guo, S., Hu, M., Wang, Z., Slanina, J., and Zhao, Y.: Size-resolved aerosol water-soluble ionic

736   compositions in the summer of Beijing: implication of regional secondary formation, Atmospheric

737   Chemistry and Physics, 10, 947-959, 2009.

738   Hallquist, M., Wenger, J., Baltensperger, U., Rudich, Y., Simpson, D., Claeys, M., Dommen, J.,

739   Donahue, N., George, C., and Goldstein, A.: The formation, properties and impact of secondary

740   organic aerosol: current and emerging issues, Atmospheric Chemistry and Physics, 9, 5155-5236,

741   2009.

742   Han, T., Liu, X., Zhang, Y., Qu, Y., Gu, J., Ma, Q., Lu, K., Tian, H., Chen, J., and Zeng, L.:

743   Characteristics of aerosol optical properties and their chemical apportionments during

744   CAREBeijing 2006, Aerosol and Air Quality Research, 14, 1431-1442, 2014.

745   Hand, J., Kreidenweis, S., Sherman, D. E., Collett, J., Hering, S., Day, D., and Malm, W.: Aerosol size

746   distributions and visibility estimates during the Big Bend regional aerosol and visibility

747   observational (BRAVO) study, Atmospheric Environment, 36, 5043-5055, 2002.

748   Hand, J. L., and Malm, W. C.: Review of the IMPROVE equation for estimating ambient light

749   extinction coefficients, CIRA, Colorado State University, 2007.

750   He, L.Y., Huang, X.F., Xue, L., Hu, M., Lin, Y., Zheng, J., Zhang, R., and Zhang, Y.H.: Submicron

751   aerosol analysis and organic source apportionment in an urban atmosphere in Pearl River Delta of

752   China using high-resolution aerosol mass spectrometry, Journal of Geophysical Research:

753   Atmospheres, 116, n/a-n/a, 10.1029/2010JD014566, 2011.

754   Ho, K., Lee, S., Chow, J. C., and Watson, J. G.: Characterization of PM_{10} and $PM_{2.5}$ source profiles for

755   fugitive dust in Hong Kong, Atmospheric Environment, 37, 1023-1032, 2003.

Atmospheric
Chemistry
and Physics
Discussions

756   Hua, Y., Cheng, Z., Wang, S., Jiang, J., Chen, D., Cai, S., Fu, X., Fu, Q., Chen, C., Xu, B., and Yu, J.:
757   Characteristics and source apportionment of $PM_{2.5}$ during a fall heavy haze episode in the Yangtze
758   River   Delta   of   China,   Atmospheric   Environment,   123,   380-391,
759   https://doi.org/10.1016/j.atmosenv.2015.03.046, 2015.
760   Huang, K., Zhuang, G., Lin, Y., Fu, J., Wang, Q., Liu, T., Zhang, R., Jiang, Y., Deng, C., and Fu, Q.:
761   Typical types and formation mechanisms of haze in an Eastern Asia megacity, Shanghai,
762   Atmospheric Chemistry & Physics, 12, 2012.
763   Huang, X., Yu, J. Z., He, L. Y., and Hu, M.: Size Distribution Characteristics of Elemental Carbon
764   Emitted from Chinese Vehicles: Results of a Tunnel Study and Atmospheric Implications,
765   Environmental Science & Technology, 40, 5355-5360, 2006a.
766   Huang, X. F., Yu, J. Z., He, L. Y., and Yuan, Z.: Water‐soluble organic carbon and oxalate in aerosols
767   at a coastal urban site in China: Size distribution characteristics, sources, and formation
768   mechanisms, Journal of Geophysical Research: Atmospheres, 111, 2006b.
769   John, W., Wall, S. M., Ondo, J. L., and Winklmayr, W.: Modes in the size distributions of atmospheric
770   inorganic aerosol, Atmospheric Environment, 24, 2349-2359, 1990.
771   Jung, J., Lee, H., Kim, Y. J., Liu, X., Zhang, Y., Gu, J., and Fan, S.: Aerosol chemistry and the effect of
772   aerosol water content on visibility impairment and radiative forcing in Guangzhou during the 2006
773   Pearl River Delta campaign, Journal of Environmental Management, 90, 3231-3244, 2009a.
774   Jung, J., Lee, H., Kim, Y. J., Liu, X., Zhang, Y., Hu, M., and Sugimoto, N.: Optical properties of
775   atmospheric aerosols obtained by in situ and remote measurements during 2006 Campaign of Air
776   Quality Research in Beijing (CAREBeijing‐2006), Journal of Geophysical Research:
777   Atmospheres (1984–2012), 114, 2009b.
778   Lan, Z., Chen, D., Li, X., Huang, X., He, L., Deng, Y., Feng, N., and Hu, M.: Modal characteristics of
779   carbonaceous aerosol size distribution in an urban atmosphere of South China, Atmospheric
780   Research, 100, 51-60, 2011.
781   Li, H., Wang, Q. g., Yang, M., Li, F., Wang, J., Sun, Y., Wang, C., Wu, H., and Qian, X.: Chemical
782   characterization and source apportionment of $PM_{2.5}$ aerosols in a megacity of Southeast China,
783   Atmospheric Research, 181, 288-299, http://doi.org/10.1016/j.atmosres.2016.07.005, 2016.
784   Lin, Z., Zhang, Z., Zhang, L., Tao, J., Zhang, R., Cao, J., Fan, S., and Zhang, Y.: An alternative method
785   for estimating hygroscopic growth factor of aerosol light-scattering coefficient: a case study in an
786   urban area of Guangzhou, South China, Atmospheric Chemistry and Physics, 14, 7631-7644,
787   2014.
788   Lowenthal, D. H., and Kumar, N.: Variation of Mass Scattering Efficiencies in IMPROVE, Journal of
789   The Air & Waste Management Association, 54, 926-934, 2004.
790   Malm, W., Sisler, J., Pitchford, M., Scruggs, M., Ames, R., Copeland, S., Gebhart, K., and Day, D.:
791   IMPROVE (interagency monitoring of protected visual environments): spatial and seasonal
792   patterns and temporal variability of haze and its constituents in the United States: Report III,
793   CIRA Report ISSN, 0737-5352, 2000.
794   Malm, W. C., Sisler, J. F., Huffman, D., Eldred, R. A., and Cahill, T. A.: Spatial and seasonal trends in
795   particle concentration and optical extinction in the United States, Journal of Geophysical Research,
796   99, 1347-1370, 1994.
797   Malm, W. C., and Pitchford, M.: Comparison of calculated sulfate scattering efficiencies as estimated
798   from size-resolved particle measurements at three national locations, Atmospheric Environment,
799   31, 1315-1325, 1997.

Atmospheric
Chemistry
and Physics
Discussions

800   Malm, W. C., Day, D. E., Kreidenweis, S. M., Collett, J. L., and Lee, T.: Humidity-dependent optical
801   properties of fine particles during the Big Bend Regional Aerosol and Visibility Observational
802   Study, Journal of Geophysical Research, 108, 4279, 2003.
803   Malm, W. C., and Hand, J. L.: An examination of the physical and optical properties of aerosols
804   collected in the IMPROVE program, Atmospheric Environment, 41, 3407-3427, 2007.
805   Ming, L., Jin, L., Li, J., Fu, P., Yang, W., Liu, D., Zhang, G., Wang, Z., and Li, X.: $PM_{2.5}$ in the Yangtze
806   River Delta, China: Chemical compositions, seasonal variations, and regional pollution events,
807   Environmental Pollution, 223, 200-212, https://doi.org/10.1016/j.envpol.2017.01.013, 2017.
808   Pitchford, M., Malm, W., Schichtel, B., Kumar, N., Lowenthal, D., and Hand, J.: Revised algorithm for
809   estimating light extinction from IMPROVE particle speciation data, Journal of the Air & Waste
810   Management Association, 57, 1326-1336, 2007.
811   Schwarz, J., Gao, R., Spackman, J., Watts, L., Thomson, D., Fahey, D., Ryerson, T., Peischl, J.,
812   Holloway, J., and Trainer, M.: Measurement of the mixing state, mass, and optical size of
813   individual black carbon particles in urban and biomass burning emissions, Geophysical Research
814   Letters, 35, 2008.
815   Seinfeld, J. H., and Pandis, S. N.: Atmospheric chemistry and physics: from air pollution to climate
816   change, John Wiley & Sons, 2012.
817   Shen, G., Xue, M., Yuan, S., Zhang, J., Zhao, Q., Li, B., Wu, H., and Ding, A.: Chemical compositions
818   and reconstructed light extinction coefficients of particulate matter in a mega-city in the western
819   Yangtze   River   Delta,   China,   Atmospheric   Environment,   83,   14-20,
820   http://dx.doi.org/10.1016/j.atmosenv.2013.10.055, 2014.
821   Shiraiwa, M., Kondo, Y., Moteki, N., Takegawa, N., Miyazaki, Y., and Blake, D. R.: Evolution of
822   mixing state of black carbon in polluted air from Tokyo, Geophysical Research Letters, 34, 2007.
823   Sisler, J. F., and Latimer, D. A.: Spatial and temporal patterns and the chemical composition of the haze
824   in the United States: An analysis of data from the IMPROVE network, 1988-1991, Cooperative
825   Institute for Research in the Atmosphere, Colorado State University, 1993.
826   Sisler, J. F., Malm, W., Gebhart, K., and Pitchford, M. L.: Spatial and Seasonal Patterns and Long Term
827   Variability of the composition of the Haze in the United States, Report ISSN, 0737-5352, 1996.
828   Sisler, J. F., and Malm, W. C.: Interpretation of Trends of PM25 and Reconstructed Visibility from the
829   IMPROVE Network, Journal of the Air & Waste Management Association, 50, 775-789, 2000.
830   Sun, J., Shen, Z., Zhang, L., Lei, Y., Gong, X., Zhang, Q., Zhang, T., Xu, H., Cui, S., Wang, Q., Cao, J.,
831   Tao, J., Zhang, N., and Zhang, R.: Chemical source profiles of urban fugitive dust PM2.5 samples
832   from 21 cities across China, Science of The Total Environment, 649, 1045-1053,
833   https://doi.org/10.1016/j.scitotenv.2018.08.374, 2019.
834   Takemura, T., Nakajima, T., Dubovik, O., Holben, B. N., and Kinne, S.: Single-Scattering Albedo and
835   Radiative Forcing of Various Aerosol Species with a Global Three-Dimensional Model, Journal of
836   Climate, 15, 333-352, 2002.
837   Tao, J., Ho, K., Chen, L., Zhu, L., Han, J., and Xu, Z.: Effect of chemical composition of $PM_{2.5}$ on
838   visibility in Guangzhou, China, 2007 spring, Particuology, 7, 68-75, 2009.
839   Tao, J., Cao, J.J., Zhang, R.J., Zhu, L., Zhang, T., Shi, S., and Chan, C.Y.: Reconstructed light
840   extinction coefficients using chemical compositions of PM 2.5 in winter in Urban Guangzhou,
841   China, Advances in Atmospheric Sciences, 29, 359-368, 2012.
842   Tao, J., Zhang, L., Cao, J., Hsu, S.C., Xia, X., Zhang, Z., Lin, Z., Cheng, T., and Zhang, R.:
843   Characterization and source apportionment of aerosol light extinction in Chengdu, southwest

844   China, Atmospheric Environment, 95, 552-562, http://dx.doi.org/10.1016/j.atmosenv.2014.07.017,
845   2014a.
846 Tao, J., Zhang, L., Ho, K., Zhang, R., Lin, Z., Zhang, Z., Lin, M., Cao, J., Liu, S., and Wang, G.:
847   Impact of $PM_{2.5}$ chemical compositions on aerosol light scattering in Guangzhou - the largest
848   megacity in South China, Atmospheric Research, 135–136, 48-58,
849   http://dx.doi.org/10.1016/j.atmosres.2013.08.015, 2014b.
850 Tao, J., Zhang, L., Gao, J., Wang, H., Chai, F., and Wang, S.: Aerosol chemical composition and light
851   scattering during a winter season in Beijing, Atmospheric Environment, 110, 36-44,
852   http://dx.doi.org/10.1016/j.atmosenv.2015.03.037, 2015.
853 Tao, J., Gao, J., Zhang, L., Wang, H., Qiu, X., Zhang, Z., Wu, Y., Chai, F., and Wang, S.: Chemical and
854   optical characteristics of atmospheric aerosols in Beijing during the Asia-Pacific Economic
855   Cooperation China 2014, Atmospheric Environment, 144, 8-16,
856   http://dx.doi.org/10.1016/j.atmosenv.2016.08.067, 2016.
857 Tao, J., Zhang, L., Cao, J., and Zhang, R.: A review of current knowledge concerning $PM_{2.5}$ chemical
858   composition, aerosol optical properties and their relationships across China, Atmos. Chem. Phys.,
859   17, 9485-9518, 10.5194/acp-17-9485-2017, 2017a.
860 Tao, J., Zhang, L., Cao, J., Zhong, L., Chen, D., Yang, Y., Chen, D., Chen, L., Zhang, Z., Wu, Y., Xia,
861   Y., Ye, S., and Zhang, R.: Source apportionment of $PM_{2.5}$ at urban and suburban areas of the Pearl
862   River Delta region, south China - With emphasis on ship emissions, Science of The Total
863   Environment, 574, 1559-1570, http://dx.doi.org/10.1016/j.scitotenv.2016.08.175, 2017b.
864 Tao, J., Zhang, Z., Tan, H., Zhang, L., Wu, Y., Sun, J., Che, H., Cao, J., Cheng, P., Chen, L., and Zhang,
865   R.: Observational evidence of cloud processes contributing to daytime elevated nitrate in an urban
866   atmosphere, Atmospheric Environment, 186, 209-215,
867   https://doi.org/10.1016/j.atmosenv.2018.05.040, 2018.
868 Tian, S., Pan, Y., Liu, Z., Wen, T., and Wang, Y.: Size-resolved aerosol chemical analysis of extreme
869   haze pollution events during early 2013 in urban Beijing, China, Journal of hazardous materials,
870   279, 452-460, 2014a.
871 Tian, S., Pan, Y., Liu, Z. X., Wen, T., and Wang, Y.: Size-resolved aerosol chemical analysis of extreme
872   haze pollution events during early 2013 in urban Beijing, China, Journal of Hazardous Materials,
873   279, 452-460, 2014b.
874 Vaughan, N. P.: The Andersen impactor: Calibration, wall losses and numerical simulation, Journal of
875   Aerosol Science, 20, 67-90, 1989.
876 Wang, H., Shi, G., Tian, M., Zhang, L., Chen, Y., Yang, F., and Cao, X.: Aerosol optical properties and
877   chemical composition apportionment in Sichuan Basin, China, Science of The Total Environment,
878   577, 245-257, http://dx.doi.org/10.1016/j.scitotenv.2016.10.173, 2017.
879 Wang, Y., Liu, Z., Zhang, J., Hu, B., Ji, D., Yu, Y., and Wang, Y.: Aerosol physicochemical properties
880   and implications for visibility during an intense haze episode during winter in Beijing,
881   Atmospheric Chemistry and Physics, 15, 3205-3215, 2014a.
882 Wang, Y., Yao, L., Wang, L., Liu, Z., Ji, D., Tang, G., Zhang, J., Sun, Y., Hu, B., and Xin, J.:
883   Mechanism for the formation of the January 2013 heavy haze pollution episode over central and
884   eastern China, Science China Earth Sciences, 57, 14-25, 2014b.
885 Watson, J. G., Chow, J. C., and Houck, J. E.: $PM_{2.5}$ chemical source profiles for vehicle exhaust,
886   vegetative burning, geological material, and coal burning in Northwestern Colorado during 1995,
887   Chemosphere, 43, 1141-1151, 2001.

Atmospheric
Chemistry
and Physics
Discussions

888   Watson, J. G.: Visibility: Science and regulation, Journal of the Air & Waste Management Association,
889   52, 628-713, 2002.
890   Watson, J. G., Chow, J. C., Lowenthal, D. H., and Magliano, K. L.: Estimating aerosol light scattering
891   at the Fresno Supersite, Atmospheric Environment, 42, 1186-1196, 2008.
892   Wu, C., and Yu, J. Z.: Determination of Primary combustion source organic carbon-to-elemental carbon
893   (OC/EC) ratio using ambient OC and EC measurements: Secondary OC-EC correlation
894   minimization method, Atmospheric Chemistry and Physics, 16, 5453-5465, 2016.
895   Wu, Y., Zhang, R., Tian, P., Tao, J., Hsu, S.C., Yan, P., Wang, Q., Cao, J., Zhang, X., and Xia, X.: Effect
896   of ambient humidity on the light absorption amplification of black carbon in Beijing during
897   January 2013, Atmospheric Environment, 124, 217-223, 2016.
898   Wu, Y., Wang, X., Tao, J., Huang, R., Tian, P., Cao, J., Zhang, L., Ho, K. F., Han, Z., and Zhang, R.:
899   Size distribution and source of black carbon aerosol in urban Beijing during winter haze episodes,
900   Atmos. Chem. Phys., 17, 7965-7975, 10.5194/acp-17-7965-2017, 2017.
901   Xia, Y., Tao, J., Zhang, L., Zhang, R., Li, S., Wu, Y., Cao, J., Wang, X., Ma, Q., and Xiong, Z.: Impact
902   of size distributions of major chemical components in fine particles on light extinction in urban
903   Guangzhou,   Science   of   The   Total   Environment,   587-588,   240-247,
904   https://doi.org/10.1016/j.scitotenv.2017.02.127, 2017.
905   Yao, T., Huang, X., He, L., Hu, M., Sun, T., Xue, L., Lin, Y., Zeng, L. M., and Zhang, Y.: High time
906   resolution observation and statistical analysis of atmospheric light extinction properties and the
907   chemical speciation of fine particulates, Science China-chemistry, 53, 1801-1808, 2010.
908   Yao, X., Lau, A. P. S., Fang, M., Chan, C. K., and Hu, M.: Size distributions and formation of ionic
909   species in atmospheric particulate pollutants in Beijing, China: 1-inorganic ions, Atmospheric
910   Environment, 37, 2991-3000, 2003.
911   Yu, H., Wu, C., Wu, D., and Yu, J.: Size distributions of elemental carbon and its contribution to light
912   extinction in urban and rural locations in the pearl river delta region, China, Atmospheric
913   Chemistry and Physics, 10, 5107-5119, 2010.
914   Zhang, F., Xu, L., Chen, J., Yu, Y., Niu, Z., and Yin, L.: Chemical compositions and extinction
915   coefficients of $PM_{2.5}$ in peri-urban of Xiamen, China, during June 2009–May 2010, Atmospheric
916   Research, 106, 150-158, 2012a.
917   Zhang, H., Wang, S., Hao, J., Wan, L., Jiang, J. S., Zhang, M., Mestl, H. E. S., Alnes, L. W. H., Aunan,
918   K., and Mellouki, A. W.: Chemical and size characterization of particles emitted from the burning
919   of coal and wood in rural households in Guizhou, China, Atmospheric Environment, 51, 94-99,
920   2012b.
921   Zhang, L., Vet, R., Wiebe, A., Mihele, C., Sukloff, B., Chan, E., Moran, M. D., and Iqbal, S.:
922   Characterization of the size-segregated water-soluble inorganic ions at eight Canadian rural sites,
923   Atmospheric Chemistry and Physics, 8, 7133-7151, 2008.
924   Zhang, R., Jing, J., Tao, J., Hsu, S. C., Wang, G., Cao, J., Lee, C. S. L., Zhu, L., Chen, Z., Zhao, Y., and
925   Shen, Z.: Chemical characterization and source apportionment of PM2.5 in Beijing: seasonal
926   perspective, Atmos. Chem. Phys., 13, 7053-7074, 10.5194/acp-13-7053-2013, 2013.
927   Zhang, R., Wang, G., Guo, S., Zamora, M. L., Ying, Q., Lin, Y., Wang, W., Hu, M., and Wang, Y.:
928   Formation of urban fine particulate matter, Chemical reviews, 115, 3803-3855, 2015a.
929   Zhang, Z., Engling, G., Zhang, L., Kawamura, K., Yang, Y., Tao, J., Zhang, R., Chan, C., and Li, Y.:
930   Significant influence of fungi on coarse carbonaceous and potassium aerosols in a tropical
931   rainforest, Environmental Research Letters, 10, 034015, 2015b.

932   Zhang, Z., Gao, J., Engling, G., Tao, J., Chai, F., Zhang, L., Zhang, R., Sang, X., Chan, C.-y., and Lin,
933   Z.: Characteristics and applications of size-segregated biomass burning tracers in China's Pearl
934   River Delta region, Atmospheric Environment, 102, 290-301, 2015c.
935   Zhao, X. J., Zhao, P. S., Xu, J., Meng, W., Pu, W., Dong, F., He, D., and Shi, Q. F.: Analysis of a winter
936   regional haze event and its formation mechanism in the North China Plain, Atmospheric
937   Chemistry and Physics, 13, 5685-5696, 2013.
938   Zheng, B., Tong, D., Li, M., Liu, F., Hong, C., Geng, G., Li, H., Li, X., Peng, L., Qi, J., Yan, L., Zhang,
939   Y., Zhao, H., Zheng, Y., He, K., and Zhang, Q.: Trends in China's anthropogenic emissions since
940   2010 as the consequence of clean air actions, Atmospheric Chemistry and Physics, 18,
941   14095-14111, 10.5194/acp-18-14095-2018, 2018.
942   Zheng, J., Zhang, L., Che, W., Zheng, Z., and Yin, S.: A highly resolved temporal and spatial air
943   pollutant emission inventory for the Pearl River Delta region, China and its uncertainty
944   assessment, Atmospheric Environment, 43, 5112-5122, 2009.
945   Zheng, M., Hagler, G. S. W., Ke, L., Bergin, M. H., Wang, F., Louie, P. K. K., Salmon, L. G., Sin, D. W.
946   M., Yu, J. Z., and Schauer, J. J.: Composition and sources of carbonaceous aerosols at three
947   contrasting sites in Hong Kong, Journal of Geophysical Research, 111, 2006.
948   Zhuang, H., Chan, C. K., Fang, M., and Wexler, A. S.: Formation of nitrate and non-sea-salt sulfate on
949   coarse particles, Atmospheric Environment, 33, 4223-4233, 1999a.
950   Zhuang, H., Chan, C. K., Fang, M., and Wexler, A. S.: Size distributions of particulate sulfate, nitrate,
951   and ammonium at a coastal site in Hong Kong, Atmospheric Environment, 33, 843-853, 1999b.
952   Zou, J., Liu, Z., Hu, B., Huang, X., Wen, T., Ji, D., Liu, J., Yang, Y., Yao, Q., and Wang, Y.: Aerosol
953   chemical compositions in the North China Plain and the impact on the visibility in Beijing and
954   Tianjin, Atmospheric Research, 201, 235-246, https://doi.org/10.1016/j.atmosres.2017.09.014,
955   2018.

Table 1 Summary of sampling information in urban Guangzhou

Season	Date	Sample type	Sampler	Sample duration	Sample number
Summer	15 July- 6 August in 2015	Size-segregated samples	Anderson 8-stage air samplers	24h	23 sets
Autumn	15 October- 5 November in 2015			24h	22 sets
Winter	4-20 January - 19-22 February in 2016			24h	21 sets
Spring	8-20 April and 4-14 May in 2016			48h	10 sets
Summer	15 July- 6 August in 2015	PM$_{2.5}$ and PM$_{10}$ samples	GSAPM	24 h	23 sets
Autumn	15 October- 5 November in 2015				22 sets
Winter	4-20 January - 19-22 February in 2016				21 sets
Spring	8-20 April and 4-14 May in 2016				20 sets

Table 2 Summary of chemical compositions concentrations in the different modes in urban Guangzhou

Chemical composition	Size mode	Annual MMAD (μm)	Annual Mass (μg m⁻³)	Spring MMAD (μm)	Spring Mass (μg m⁻³)	Summer MMAD (μm)	Summer Mass (μg m⁻³)	Autumn MMAD (μm)	Autumn Mass (μg m⁻³)	Winter MMAD (μm)	Winter Mass (μg m⁻³)
PM	Condensation	0.21±0.00	5.7±2.3 (10±2%)	0.21±0.00	6.6±3.0 (10±3%)	0.21±0.00	4.0±1.3 (8±1%)	0.21±0.00	7.0±1.9 (10±2%)	0.21±0.00	5.7±2.2 (10±2%)
	Droplet	0.78±0.07	29.1±11.8 (48±7%)	0.87±0.13	31.9±8.7 (50±8%)	0.78±0.05	20.4±8.0 (42±8%)	0.79±0.05	35.6±9.7 (46±4%)	0.79±0.05	30.6±13.2 (52±5%)
	Coarse	4.57±0.42	25.5±10.1 (42±8%)	4.37±0.37	25.3±7.0 (40±7%)	4.47±0.35	23.1±4.9 (50±7%)	4.47±0.24	30.8±11.8 (44±6%)	4.47±0.24	22.5±11.7 (38±6%)
SO₄²⁻	Condensation	0.21±0.00	1.0±0.5 (12%)	0.21±0.00	0.9±0.3 (10%)	0.21±0.00	0.9±0.3 (15%)	0.21±0.00	1.4±0.5 (13%)	0.21±0.00	0.6±0.3 (10%)
	Droplet	0.80±0.08	6.5±2.9 (77%)	0.86±0.07	7.3±2.3 (79%)	0.79±0.07	4.9±2.6 (75%)	0.77±0.08	8.5±2.6 (75%)	0.82±0.08	5.8±2.7 (79%)
	Coarse	4.17±0.44	0.9±0.6 (11%)	4.34±0.59	0.9±0.6 (11%)	4.09±0.16	0.6±0.3 (10%)	4.08±0.22	1.4±0.8 (12%)	4.20±0.59	0.8±0.5 (11%)
NO₃⁻	Condensation	0.21±0.00	0.4±0.3 (10%)	0.21±0.00	0.4±0.2 (6%)	0.21±0.00	0.2±0.2 (9%)	0.21±0.00	0.4±0.3 (10%)	0.21±0.00	0.6±0.3 (13%)
	Droplet	0.85±0.21	2.2±2.2 (46%)	0.87±0.07	3.2±2.1 (51%)	0.94±0.35	0.8±0.5 (35%)	0.80±0.09	2.1±1.7 (39%)	0.80±0.07	3.2±2.9 (63%)
	Coarse	4.38±0.61	1.8±1.4 (44%)	4.47±0.62	2.4±1.2 (43%)	4.15±0.52	1.3±0.7 (56%)	4.36±0.31	2.4±1.7 (51%)	4.74±0.76	1.3±1.5 (24%)
NH₄⁺	Condensation	0.21±0.00	0.2±0.2 (6%)	0.21±0.00	0.2±0.1 (6%)	0.21±0.00	0.1±0.1 (5%)	0.21±0.00	0.2±0.2 (7%)	0.21±0.00	0.2±0.2 (6%)
	Droplet	0.76±0.13	2.4±1.5 (89%)	0.86±0.17	2.8±1.1 (89%)	0.70±0.11	1.4±1.1 (91%)	0.73±0.12	3.1±1.4 (90%)	0.82±0.10	2.5±1.7 (86%)
	Coarse	3.25±0.69	0.1±0.1 (5%)	3.13±1.16	0.2±0.2 (6%)	3.36±0.68	0.0±0.0 (4%)	3.01±0.23	0.1±0.1 (3%)	3.45±0.70	0.2±0.1 (8%)
OC	Condensation	0.21±0.00	1.2±0.6 (13±4%)	0.21±0.00	1.4±0.4 (19±4%)	0.21±0.00	0.8±0.3 (11±4%)	0.21±0.00	1.6±0.5 (14±2%)	0.21±0.00	1.2±0.6 (13±4%)
	Droplet	0.76±0.07	5.5±2.4 (62±9%)	0.73±0.06	3.9±1.6 (51±6%)	0.77±0.07	4.1±1.3 (63±9%)	0.75±0.08	6.9±2.0 (58±5%)	0.78±0.06	6.5±2.6 (69±7%)
	Coarse	3.73±0.58	2.2±1.1 (25±8%)	3.99±0.25	2.2±0.7 (30±3%)	3.50±0.73	1.7±0.9 (26±9%)	3.44±0.39	3.3±1.3 (28±4%)	3.44±0.39	1.7±0.9 (18±8%)
EC	Condensation	0.21	0.1±0.1 (11%)	0.21±0.00	0.1±0.0 (9%)	0.21±0.00	0.0±0.0 (5%)	0.21±0.00	0.1±0.1 (16%)	0.21±0.00	0.1±0.0 (11%)
	Droplet	0.66±0.08	2.0±1.0 (55±7%)	0.65±0.08	1.8±0.8 (54±9%)	0.61±0.08	1.3±0.5 (50±5%)	0.71±0.04	2.7±0.9 (62±6%)	0.67±0.07	2.1±0.9 (54±5%)
	Coarse	3.69±0.65	0.5±0.3 (14±7%)	3.54±0.61	0.3±0.2 (10±6%)	3.48±0.52	0.5±0.3 (18±6%)	4.17±0.24	0.6±0.2 (14±5%)	3.50±0.75	0.4±0.3 (11±8%)
Na⁺	Condensation	0.21±0.00	0.1±0.1 (11%)	0.21±0.00	0.1±0.0 (9%)	0.21±0.00	0.0±0.0 (5%)	0.21±0.00	0.1±0.1 (16%)	0.21±0.00	0.1±0.0 (11%)
	Droplet	0.86±0.12	0.4±0.2 (48%)	0.84±0.10	0.3±0.0 (48%)	0.96±0.11	0.4±0.1 (45%)	0.81±0.09	0.4±0.3 (52%)	0.80±0.11	0.3±0.2 (48%)
	Coarse	3.75±0.38	0.4±0.3 (41%)	3.90±0.63	0.3±0.2 (43%)	3.60±0.19	0.6±0.4 (50%)	3.64±0.27	0.3±0.3 (32%)	3.94±0.38	0.3±0.2 (41%)
K⁺	Condensation	0.21±0.00	0.1±0.0 (13%)	0.21±0.00	0.0±0.0 (10%)	0.21±0.00	0.1±0.0 (16%)	0.21±0.00	0.1±0.0 (12%)	0.21±0.00	0.1±0.0 (12%)
	Droplet	0.69±0.08	0.3±0.2 (78%)	0.76±0.07	0.3±0.1 (76%)	0.64±0.08	0.3±0.1 (72%)	0.67±0.07	0.4±0.2 (87%)	0.73±0.06	0.4±0.2 (77%)
	Coarse	3.74±0.51	0.0±0.0 (9%)	3.94±0.40	0.1±0.0 (14%)	3.74±0.64	0.0±0.0 (12%)	3.30±0.38	0.0±0.0 (1%)	3.78±0.35	0.0±0.0 (11%)
Ca²⁺	Condensation	0.21±0.00	0.0±0.0 (4%)	0.21±0.00	0.1±0.0 (7%)	0.21±0.00	0.0±0.0 (4%)	0.21±0.00	0.1±0.1 (3%)	0.21±0.00	0.0±0.0 (5%)
	Droplet	0.91±0.12	0.2±0.1 (24%)	0.88±0.13	0.3±0.1 (36%)	1.00±0.11	0.3±0.1 (30%)	0.81±0.10	0.2±0.1 (16%)	0.92±0.09	0.2±0.1 (21%)
	Coarse	4.57±0.54	0.8±0.4 (72%)	5.02±0.58	0.6±0.2 (57%)	4.10±0.42	0.7±0.3 (66%)	4.72±0.47	1.1±0.5 (81%)	4.73±0.38	0.7±0.3 (74%)
Cl⁻	Condensation	0.21±0.00	0.0±0.0 (5%)	0.21±0.00	0.1±0.0 (5%)	0.21±0.00	0.0±0.0 (2%)	0.21±0.00	0.1±0.0 (5%)	0.21±0.00	0.0±0.0 (10%)
	Droplet	0.89±0.13	0.2±0.3 (24%)	0.89±0.10	0.7±0.7 (37%)	0.92±0.20	0.0±0.0 (9%)	0.89±0.05	0.0±0.0 (17%)	0.85±0.08	0.2±0.2 (42%)
	Coarse	3.77±0.35	0.4±0.4 (71%)	3.97±0.12	0.8±0.4 (58%)	3.70±0.23	0.4±0.3 (89%)	3.72±0.21	0.3±0.2 (78%)	3.80±0.50	0.4±0.6 (48%)

Atmospheric
Chemistry
and Physics
Discussions
Open Access

Table 3 Summary of the estimated MSEs of particle and the dominant chemical species in urban Guangzhou

Chemical species	Size mode	Annual MMAD (µm)	Annual MSE ($m^2 g^{-1}$)	Spring MMAD (µm)	Spring MSE ($m^2 g^{-1}$)	Summer MMAD (µm)	Summer MSE ($m^2 g^{-1}$)	Autumn MMAD (µm)	Autumn MSE ($m^2 g^{-1}$)	Winter MMAD (µm)	Winter MSE ($m^2 g^{-1}$)
PM*	Condensation	0.21±0.00	2.1±0.2	0.21±0.00	1.9±0.2	0.21±0.00	2.0±0.1	0.21±0.00	2.1±0.1	0.21±0.00	2.2±0.2
	Droplet	0.78±0.07	4.3±0.2	0.87±0.13	4.0±0.1	0.78±0.05	4.2±0.1	0.74±0.06	4.3±0.2	0.79±0.05	4.4±0.2
	Coarse	4.57±0.42	0.5±0.0	4.37±0.37	0.6±0.1	4.47±0.35	0.5±0.0	4.90±0.46	0.5±0.0	4.47±0.24	0.5±0.0
	Fine mode**	3.7±0.2		3.5±0.1		3.6±0.2		3.8±0.2		3.9±0.2	
(NH₄)₂SO₄	Condensation	0.21±0.00	2.1±0.5	0.21±0.00	1.9±0.6	0.21±0.00	2.6±0.2	0.21±0.00	2.0±0.5	0.21±0.00	1.9±0.5
	Droplet	0.79±0.17	4.7±0.6	0.92±0.13	4.3±0.3	0.74±0.20	4.8±0.6	0.72±0.16	4.9±0.7	0.84±0.13	4.6±0.7
	Fine mode	4.4±0.8		4.1±0.4		4.5±0.6		4.6±0.8		4.3±0.9	
NH₄NO₃	Condensation	0.21±0.00	2.3±0.8	0.21±0.00	2.0±0.8	0.21±0.00	2.9±0.3	0.21±0.00	2.6±1.0	0.21±0.00	2.3±0.7
	Droplet	0.80±0.16	4.8±0.9	0.90±0.18	4.5±0.8	0.77±0.17	4.9±0.8	0.75±0.13	5.1±1.0	0.82±0.14	4.7±0.8
	Fine mode	4.5±1.5		4.2±1.2		4.7±0.9		4.9±2.0		4.4±1.3	
OM	Condensation	0.21±0.00	2.7±0.1	0.21±0.00	2.5±0.1	0.21±0.00	2.8±0.2	0.21±0.00	2.6±0.1	0.21±0.00	2.8±0.1
	Droplet	0.76±0.07	5.3±0.2	0.73±0.06	5.4±0.1	0.77±0.07	5.2±0.2	0.78±0.06	5.3±0.2	0.75±0.08	5.5±0.2
	Coarse	3.73±0.58	0.8±0.1	3.99±0.25	0.8±0.0	3.50±0.73	0.8±0.1	4.14±0.24	0.7±0.0	3.44±0.39	0.8±0.1
	Fine mode	4.6±0.3		4.4±0.2		4.6±0.2		4.5±0.1		4.9±0.3	
EC	Condensation	0.21±0.00	2.9±0.1	0.21±0.00	2.9±0.1	0.21±0.00	2.9±0.1	0.21±0.00	3.0±0.1	0.21±0.00	2.9±0.1
	Droplet	0.66±0.08	2.3±0.2	0.65±0.08	2.3±0.2	0.61±0.08	2.3±0.2	0.71±0.04	2.2±0.1	0.67±0.07	2.3±0.2
	Coarse	3.69±0.65	0.4±0.0	3.54±0.61	0.4±0.0	3.48±0.52	0.4±0.0	4.17±0.24	0.4±0.0	3.50±0.75	0.5±0.0
	Fine mode	2.6±0.1		2.6±0.1		2.6±0.2		2.5±0.1		2.6±0.1	
Crustal element oxides	Condensation	0.21±0.00	0.7±0.0	0.21±0.00	0.7±0.0	0.21±0.00	0.7±0.1	0.21±0.00	0.7±0.0	0.21±0.00	0.7±0.0
	Droplet	0.91±0.12	2.9±0.2	0.88±0.13	3.0±0.2	1.00±0.11	2.9±0.2	0.81±0.10	2.8±0.2	0.92±0.09	2.8±0.2
	Coarse	4.57±0.54	0.4±0.0	5.02±0.58	0.4±0.0	4.10±0.42	0.5±0.0	4.72±0.47	0.4±0.0	4.73±0.38	0.4±0.0
	Fine mode	2.4±0.2		2.4±0.1		2.5±0.2		2.4±0.2		2.3±0.2	
Unidentified	Condensation	0.21±0.00	1.3±0.2	0.21±0.00	1.2±0.4	0.21±0.00	1.2±0.2	0.21±0.00	1.4±0.1	0.21±0.00	1.3±0.2
	Droplet	0.85±0.26	3.8±0.6	1.00±0.20	3.5±0.8	0.74±0.44	3.9±0.9	0.84±0.10	3.9±0.2	0.90±0.20	3.7±0.4
	Coarse	5.74±1.52	0.4±0.1	4.55±0.71	0.5±0.1	6.46±1.14	0.4±0.1	6.33±1.62	0.4±0.1	4.91±0.90	0.5±0.1
	Fine mode	3.1±0.8		2.9±0.9		2.6±1.0		3.3±0.3		3.1±0.5	
NaCl	Coarse	4.88±0.41	0.5±0.1	5.14±0.70	0.5±0.1	4.49±0.38	0.6±0.0	5.38±0.43	0.5±0.0	4.66±0.65	0.5±0.0

*PM: Particulate matter; **Fine mode = sum of condensation and droplet modes

Atmospheric
Chemistry
and Physics
Discussions

Open Access

List of Figures

Fig. 1. The sampling locations in urban Guangzhou in the PRD region of China.

Atmospheric
Chemistry
and Physics
Discussions

Open Access

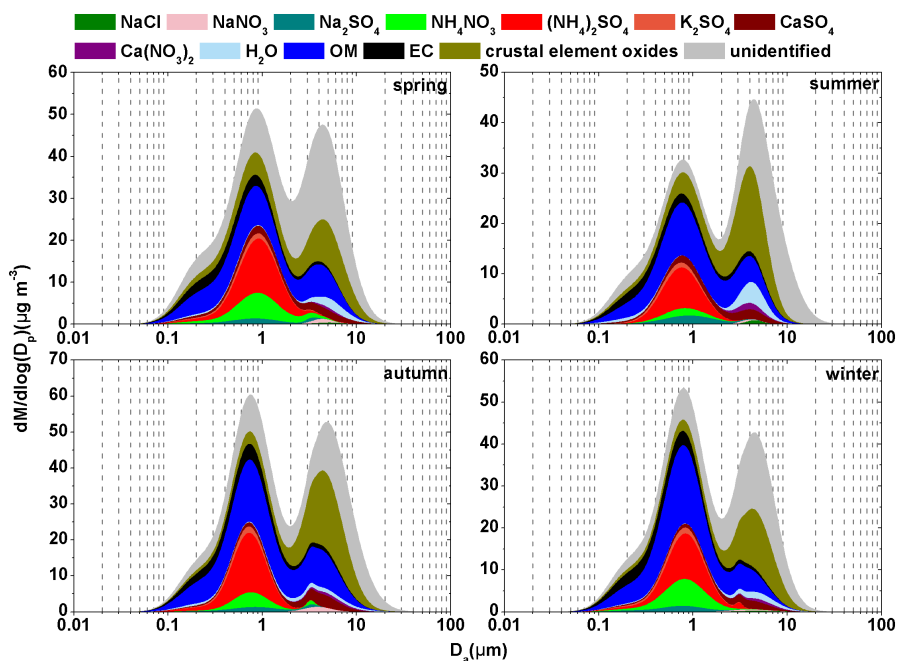Fig. 2. Continuous log-normal size distributions of chemical species mass concentrations in four seasons (dlogD$_a$=0.01μm).

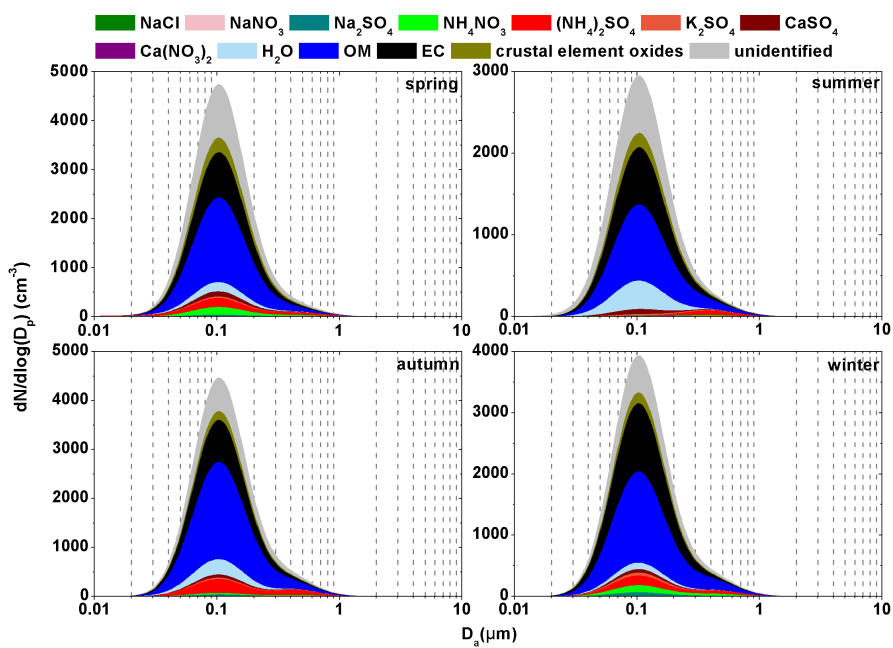Fig. 3. Continuous log-normal size distributions of the estimated chemical species number concentrations in four seasons (dlogD$_a$=0.01μm).

Atmospheric
Chemistry
and Physics
Discussions
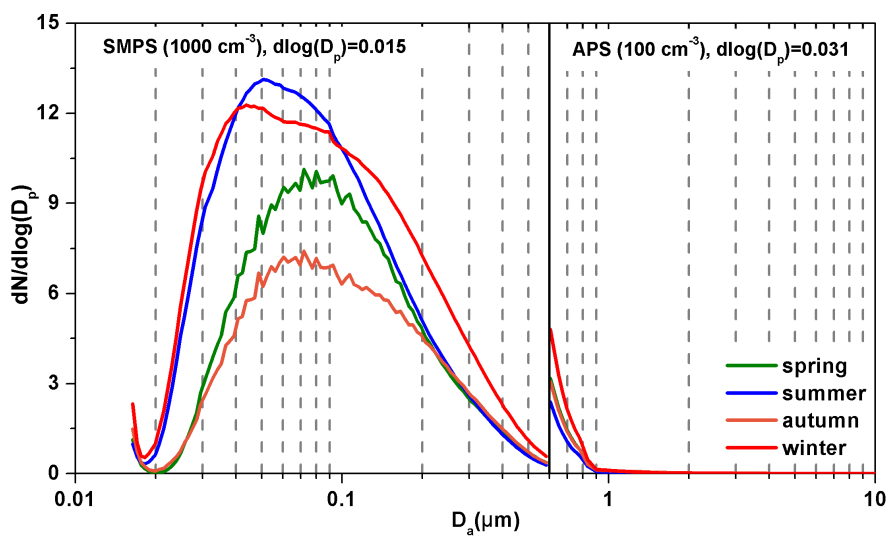
Fig. 4. Continuous log-normal size distributions of the measured particle number
concentrations in four seasons.

Atmospheric
Chemistry
and Physics
Discussions

Open Access

EGU
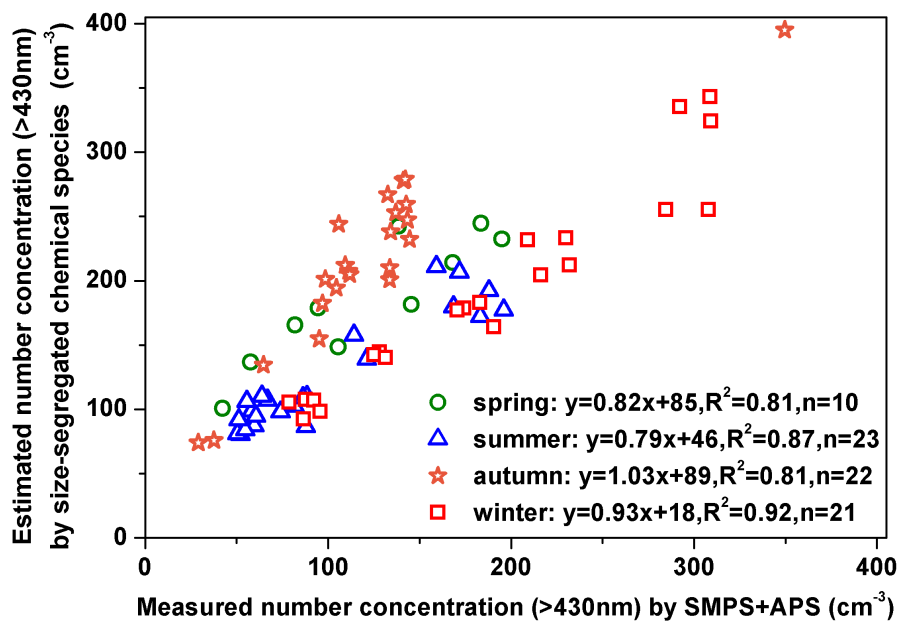
Fig. 5. Correlations between the estimated and SMPS- and APS-measured particle number concentrations in four seasons.

Atmospheric
Chemistry
and Physics
Discussions

Open Access
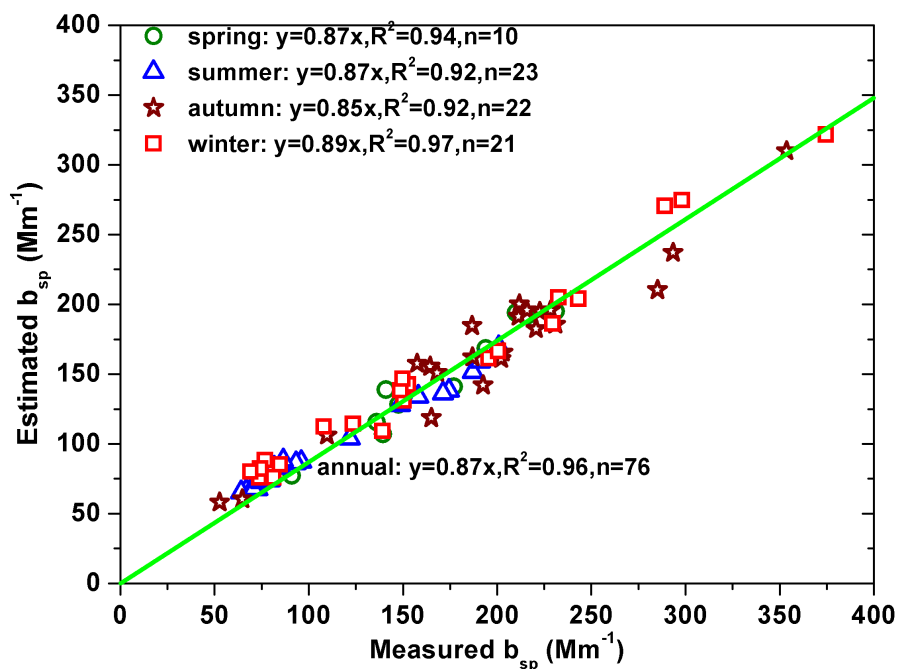
Fig. 6. Correlations between the measured and estimated b_{sp} in four seasons.

Atmospheric
Chemistry
and Physics
Discussions
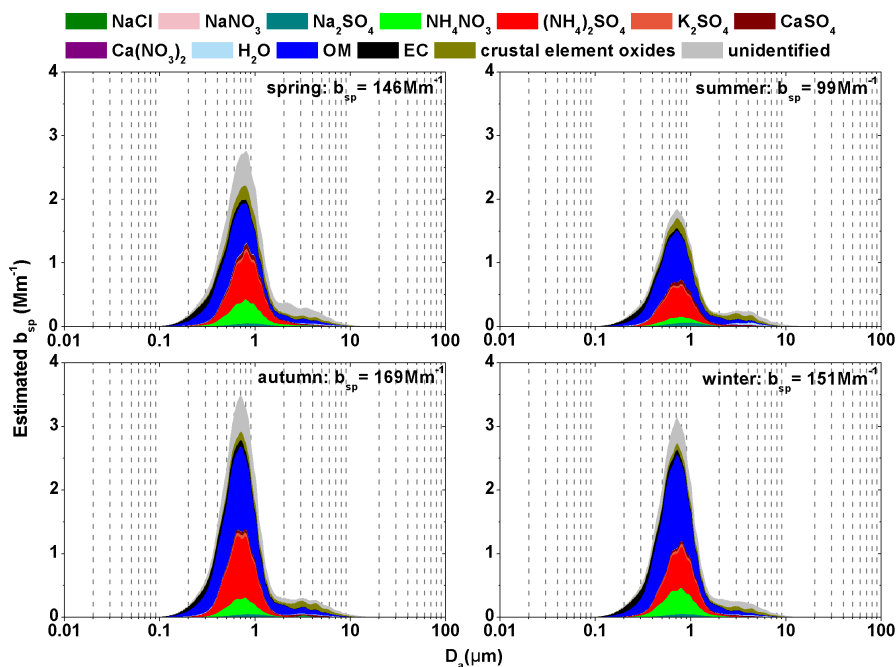
Fig. 7. The contributions of continuous log-normal size distributions of chemical species on the estimated b_{sp} in four seasons (dlogD$_a$=0.01μm).
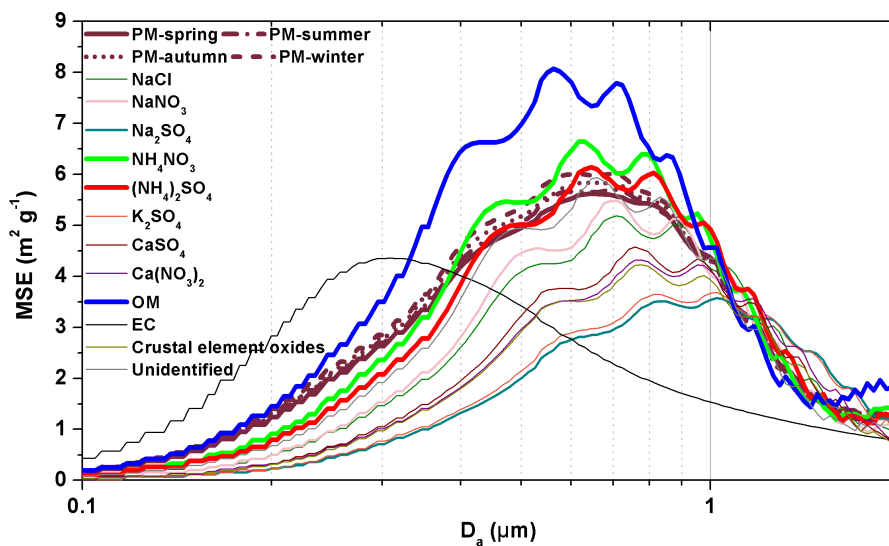
Fig. 8. Continuous log-normal size distributions of fine particle MSEs in four seasons and the MSEs of chemical species.
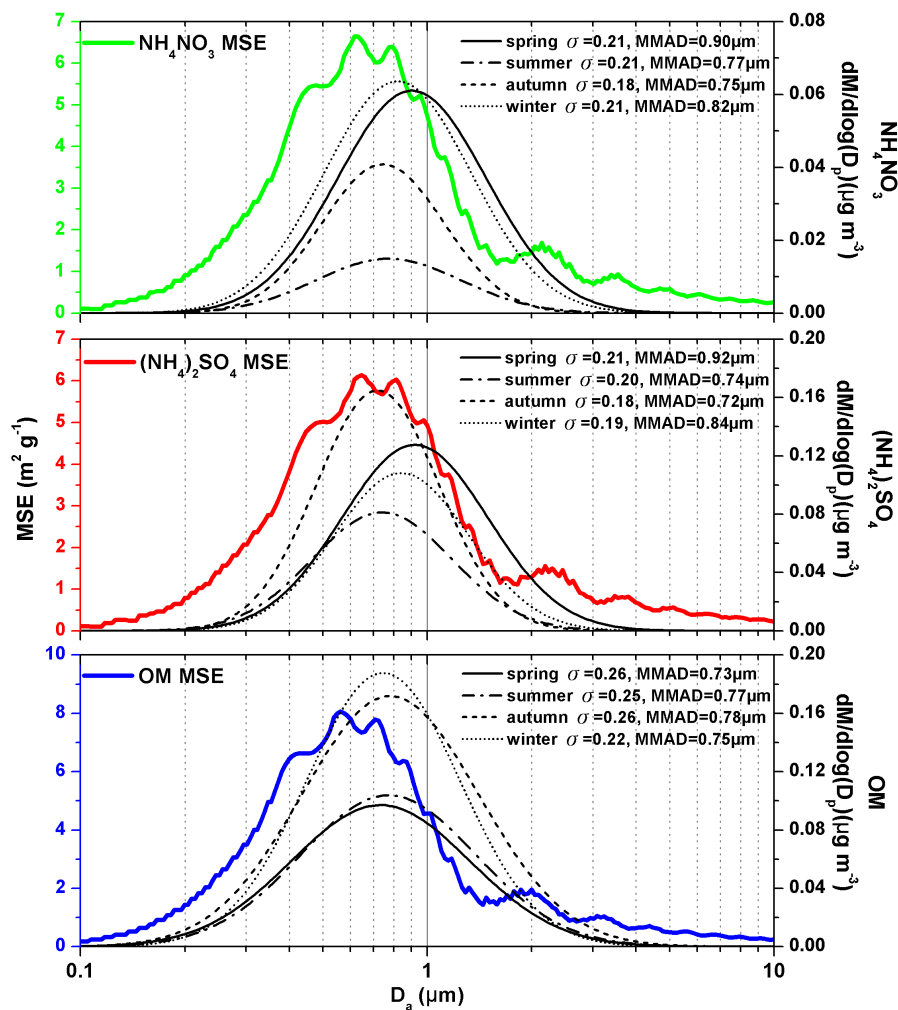
Atmospheric
Chemistry
and Physics
Discussions

Fig. 9. Continuous log-normal size distributions of (NH$_4$)$_2$SO$_4$ (a), NH$_4$NO$_3$ (b) and

OM (c) mass concentrations and their σ values and MMADs in the droplet mode.